Available online at www.sciencedirect.com
SCIENCE DIRECT®
Progress in Oceanography 62 (2004) 33–66
Progress in Oceanography
www.elsevier.com/locate/pocean

Annual and decadal variability in the western subtropical North Atlantic: signal characteristics and sampling methodologies

Robert L. Molinari *

National Oceanic and Atmospheric Administration, Atlantic Oceanographic and Meteorological Laboratory, 4301 Rickenbacker Causeway, Miami, FL 33149, USA

Received 17 October 2003; received in revised form 24 May 2004; accepted 14 July 2004
Available online 24 August 2004

Abstract

Upper ocean (above 750 m) temperature structure of the northwestern subtropical Atlantic, including the Gulf Stream and a recirculation gyre south of the Stream, is characterized using primarily bathythermograph (BT) data collected between 1950 and 2003. Geostrophic calculations, using mean temperature–salinity relationships to compute dynamic height, are used to estimate velocities and transports. The mean annual Gulf Stream transport at 72° W relative to 750 m, 36.1 Sv, is approximately equal to the sum of the transport of the Florida Current, 32.0 Sv, and a shallow recirculation gyre described by Wang and Koblinsky [Journal of Physical Oceanography 26 (1996) 2462–2479], 5.5 Sv. The annual cycle of geostrophic transport relative to 750 m at 72° W is in phase with both an earlier published annual cycle of transport relative to 2000 m derived from hydrographic observations and the annual cycle of Florida Current transport measured indirectly by a submarine cable (i.e., maximum transports are observed in the summer and minimum in the fall, early winter). However, simple Sverdrup dynamics are inadequate to explain these cycles as maximum Sverdrup transports extend from winter to summer, while observed transports are minimum (maximum) in fall/winter (summer). The annual cycles derived from the BT data of the size of the shallow southern recirculation gyre, Gulf Stream position and upper layer transport (relative to 300 m) are in phase (maximum size, northern position and transport in fall) and consistent with the WK results derived from altimetry. However, the shallower annual cycles are out of phase with the deeper signals (i.e., maximum for the former (latter) are observed in fall (summer)). Decadal signals after 1965 in Gulf Stream position, geostrophic transport relative to 450 m, and the size of a recirculation gyre south of the Stream are approximately in phase as observed for the annual signal. This gyre and the shallow WK gyre exhibit the same horizontal structure, however, the decadal signal propagates deeper into the water column (at least to

* Tel.: +1 305 361 4344; fax: +1 305 361 4392.
E-mail address: bob.molinari@noaa.gov.

0079-6611/$ - see front matter. Published by Elsevier Ltd.
doi:10.1016/j.pocean.2004.07.002

700 m). The eastern expansion and contraction of the gyre on decadal time-scales is correlated with propagating SST signals. The sampling implications of these findings are addressed.
Published by Elsevier Ltd.

Keywords: Gulf stream; Recirculation gyre; Annual period; Decadal period; North Atlantic oscillation; Sampling

1. Introduction

Many recent research studies have been directed at decadal and multidecadal modes of sea-surface temperature (SST) variability in the North Atlantic Ocean and the possible role of these modes in the forcing of atmospheric climate anomalies at similar periods. The earlier observational and modeling studies have addressed several basic questions about these signals including: is variability at these time-scales a product of coupled air–sea interaction, the atmosphere driving the ocean and/or the ocean driving the atmosphere; does the subsurface ocean participate in this variability and, if so, what drives the oceanic anomalies (e.g., surface heat fluxes, wind-stress curl, etc.); and are mid-latitude SST anomalies a factor in climate?

The possibility of subsurface oceanic features contributing to longer period SST anomalies requires consideration of such phenomena as the Gulf Stream, the subtropical and subpolar gyres, recirculation gyres north and south of the Stream, and the Deep Western Boundary Current (DWBC). For example, only a 100 km meridional shift in Gulf Stream position can cause local SST changes of greater than 2 °C in the western Atlantic. Changes in Gulf Stream position of this amplitude have been observed. On short time-scales these changes have been attributed to Stream meanders and on long time-scales, to variability in both the North Atlantic gyres and the DWBC.

The North Atlantic oscillation (NAO), an atmospheric teleconnection pattern has been the focus of many air–sea interaction studies involving, for example, the time-dependent characteristics of the subtropical gyre of the North Atlantic and the Gulf Stream. The questions posed above relative to air–sea coupling are all relevant to the role of the NAO in climate variability at decadal and longer periods.

Less attention has been directed at the development of the ocean observing systems needed to provide sustained and cost-effective characterizations of longer timescale climate variability. The data provided by such systems are also needed, for example, to evaluate: the role of the ocean in global carbon dioxide budgets; the effect of oceanic anomalies on marine ecosystems; sea level rise, etc. Thus, even if additional research determines that the ocean is only responding to atmospheric anomalies, the societal importance of these other issues requires more accurate oceanic forecasts and the ocean observing system needed to support these forecasts. Therefore, in the following, not only will the characteristics of the annual and decadal signals in the subtropical North Atlantic and their relation to atmospheric anomalies be considered but the implications of the oceanic characteristics at these time-scales for sustained observing systems will also be addressed.

Herein, we use temperature data derived primarily from bathythermographs (BT's) to characterize the variability of the Gulf Stream and the subtropical and recirculation gyres at decadal time-scales. The relationship of these oceanic signals to decadal signals in atmospheric variables is also addressed. Results from various models are used to search for dynamical mechanisms that could explain the anomalous behavior in both media.

Consideration is also given to the annual cycle of these features. Definition and removal of the annual cycle are typically the first steps in characterizing decadal signals in a gappy time series in which the amplitude of the former is large compared to the amplitude of the latter. By first removing the annual cycle from the gappy records, the potential for aliasing of the lower frequency signal is reduced. Characterizations of the annual cycle of various features in the western subtropical Atlantic are described to provide insight into the causes of variability at this period.

Previous research on decadal signals in the Atlantic is reviewed in Section 2. The evolution of the BT networks will then be described. A new profiling float technology will also be discussed as an evolutionary step in observing upper ocean temperature and salinity properties. This section will be followed by a description of the analytical methods used on the data. Section 5 will include comparisons of time series depicting annual and decadal signals of several Gulf Stream and recirculation gyre properties derived from BT's to similar time series derived from other sources and to potential forcing mechanisms. The comparisons will demonstrate the ability of the BT data to resolve annual and decadal signals in the subtropical Atlantic. Sampling implications of the characteristics of the annual and decadal signals will complete the results section. A discussion of the relation of these results to previous studies with particular attention directed at possible cause and effect relationships and implications of the findings to future observing systems will conclude the paper.

2. Background

2.1. Observational studies

Observationally, decadal signals have been identified in surface and subsurface oceanic features of the western subtropical Atlantic that might be coupled to atmospheric anomalies. Unfortunately, the oceanographic observations used in the earlier studies of coupled air–sea interactions at these longer time-scales were limited primarily to sea-surface temperature (SST) data because of the paucity of subsurface data. The instrumental SST record is somewhat longer than 150 years, while the subsurface record is typically at most 50–60 years long. Thus, even in the SST records, at most 10–15 cycles of any decadal modes can be resolved.

In addition to the problem of short records, the studies of longer time-scales have to deal with changes in instrumentation. For instance, early observations of SST were typically based on water samples collected from buckets. After World War II, SST was primarily measured using engine intake samples. Methods have been developed to compensate for these changes and the resulting temperature signals that might result from different instrumentation (e.g., see the discussion in Deser & Blackmon (1994) describing an increase in SST around 1940). A method for combining MBT's and XBT's taken from Kessler (1990) will be used in the present study. In this approach anomalies are calculated relative to means generated for each BT type rather than from a combination of both BTs.

Surprisingly, in view of these data limitations, many of the earlier studies of surface and subsurface ocean variability frequently concentrated on multidecadal rather than decadal signals. For example, Bjerknes (1964) addressed multidecadal periods in SST and sea level pressure, SLP, using the instrumental record. He hypothesized that at these frequencies, the atmosphere was responding to changes in the Gulf Stream system and the resulting advection of SST anomalies (i.e., wind driven effects). Alternatively, Kushnir (1994) attributed multidecadal SST and SLP anomalies to variability in the thermohaline circulation. Delworth and Mann (2000) used paleoclimatic data to extend the SST record to the mid-1600s and found signals in the 60–100 year band. They also attributed the SST anomalies to variability in the thermohaline circulation.

Studies of decadal time-scales also suggest that different modes of air sea interaction could be active. For example, Deser and Blackmon (1994) used an EOF analysis to identify the spatial and temporal characteristics of SST and SLP variability at these periods. They argued that the decadal SST mode in the subtropics is merely a local response to wind stress anomalies associated with the NAO.

Building on the Bjerknes (1964) hypothesis that anomalies in North Atlantic gyre structure affect SST and thus SLP patterns, several observational studies have considered the properties of the Gulf Stream as it separates from the coast. Modeling studies indicate that this is a potential area for coupled mid-latitude air–sea

interactions (e.g., Battisti, Bhatt, & Alexander, 1995). Joyce, Deser, and Spall (2000), hereinafter JDS, defined the location of the axis of the Gulf Stream as the position of the 15 °C isotherm at 200 m (i.e., a depth relatively independent of surface diabatic processes). JDS performed an EOF analysis of the Gulf Stream position at nine locations between 75° W and 55° W. They found that along this path the Gulf Stream oscillates meridionally with a decadal period. However, when considering the details of the variability, they constructed 5-year pentads because of data limitations. Using the pentads, they went on to suggest that these Gulf Stream oscillations through their effect on SST can have a significant impact on storms that cross the Atlantic. Because of the zero time lag between Gulf Stream oscillations and NAO anomalies, they argue that the signals in the two media are coupled.

Intense recirculation gyres have been identified north and south of the Gulf Stream. Early studies of the southern gyre demonstrated that it occupies the total water column and contributes to large increases in Gulf Stream transport as it separates from the western boundary (e.g., Stommel, Niiler, & Anati, 1978, Hogg, 1992, Curry & McCartney, 2001, hereinafter CM). The baroclinic component of this gyre appears in the dynamic height field of the western Atlantic on the southern flank of the Gulf Stream (Fig. 1).

Recent studies have characterized temporal and spatial variability of the southern gyre that can have an impact on the properties of the Gulf Stream. For instance, Kelly, Caruso, Singh, and Qiu (1996) used 2.5 years of satellite altimetry data from Geosat combined with surface forcing fields to address the question of the relative importance of surface fluxes and wind stress curl on the structure of the Gulf Stream and southern recirculation gyre. They found west of 62° W on 5–9 month time-scales that anomalous surface cooling was correlated with weaker (southerly) Gulf Stream transport (position). The cooling reduced the SST gradient across the Stream and thereby, the surface geostrophic transport of the boundary flow. Because of the amplitude of the transport change (approaching the transport of the western boundary current), they argue that these anomalies are related to anomalies in the size of the southern recirculation gyre. The gyre was smaller during the time of cooling. The time-scales of these correlations included a trend over the 2.5 years of Geosat data (Fig. 1) as well as the 5–9 month peak in variability. On the longer time-scale, they also found evidence for a relationship between the tilt of the zero wind stress curl line and the size of the southern gyre. The more tilted the line, the shorter the southern gyre.

Similarly, using satellite altimetry data, Wang and Koblinsky (1996), WK, identified a recirculation gyre located within and south of the Gulf Stream that is limited to the upper layers but overlies both the total water column gyre and Kelly et al. (1996) features (Fig. 1). The WK feature is characterized temporally by an annual signal in the size of the gyre. The gyre has greatest eastward extent in the fall, and least in spring. WK found these changes to be correlated with the annual signal of upper layer Gulf Stream transports, as determined by altimetry, with transports greater (smaller) in fall (spring). They also found a similar signal in Gulf Stream position, with the Stream farthest north (south) in fall (spring). Thus, the annual cycle of shallow gyre size is in phase with Gulf Stream transport and position as found by Kelly et al. (1996) for somewhat different time-scales.

Considering longer time-scales, CM generated a Gulf Stream/North Atlantic Current transport index using time series of hydrographic data available at Bermuda and the Labrador Sea (see Fig. 1 for station locations). They noted that the records available for their study included some suggestion of decadal signals but were inadequate to characterize quantitatively variability at this period. They concentrated on a multi-decadal signal with a minimum (southerly position) in Gulf Steam transport (latitude) in 1964–1970 and a maximum (northerly position) in 1990–1997.

CM generated regional distributions of potential energy anomaly (PEA, the vertical integral of specific volume anomaly multiplied by pressure) of the 200-db surface relative to 2000 db for the extreme years of Gulf Stream transport (and position). A PEA difference map between these periods demonstrated that the extremes in transport and position anomalies were coincident with changes in the size of the WK recirculation gyre (Fig. 1). Similarly, the CM gyre extends farthest (least) eastward when the Stream is strong (weak) and at it's northernmost (southernmost) position as described by WK for the annual signal. CM

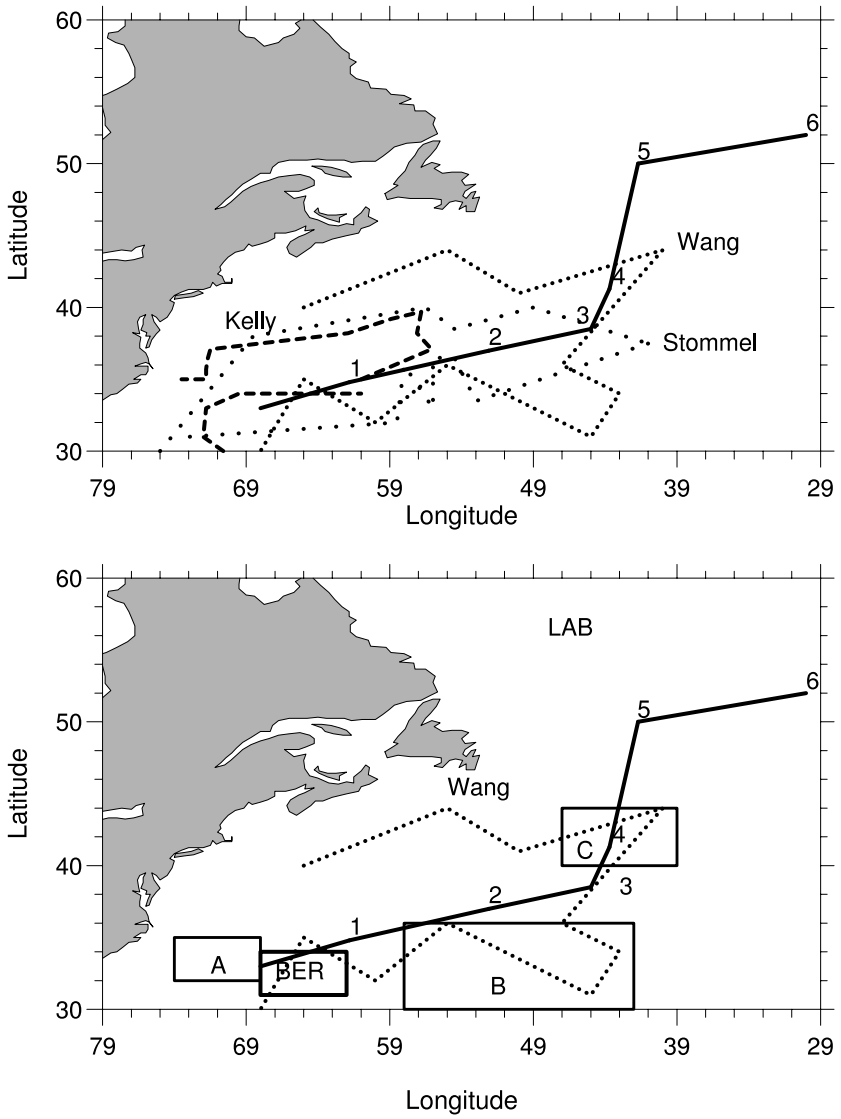

Fig. 1. Upper panel: The shallow recirculation gyre derived from the EOF analysis of satellite altimetry data by Wang and Koblinsky (1996), Wang, closely spaced dots: the extended recirculation gyre of Kelly et al. (1996), Kelly, dashed line; the 680 dynamic millimeter contour from the dynamic topography of the 1500 db surface relative to 3000 db from Stommel et al. (1978), Stommel, widely spaced dots. The solid line represents the path of the center of areas of maximum SST correlation with SST at the start of the line. Numbers indicate year from the start of the line. Bottom panel: The Wang and Koblinsky (1996) and the line of maximum SST correlations from the upper panel. Quadrangles A, B and C are those described in Curry and McCartney (2001) as regions of maximum increases in potential energy anomalies between years of maximum and minimum Gulf Stream transport. Temperature data from quadrangle BER that includes Bermuda is used in place of temperature data from A in the text. LAB and BER represent the approximate location of the hydrographic stations used by Curry and McCartney (2001) to estimate Gulf Stream/North Atlantic Current transport.

found that in the eastern portion of the recirculation gyre (box C, Fig. 1) the largest changes in PEA occurred between 500 and 1200 db (i.e., in the main thermocline). Thus, the CM gyre extends deeper and has longer time-scale variability than the shallower WK gyre but similar correlations with Gulf Stream transport and position.

Finally, several studies have identified SST signals that propagate along the path of the Gulf Stream and North Atlantic Current. In particular, Sutton and Allen (1997), SA, using observations, tracked SST anomalies from the Straits of Florida to the North Sea (Fig. 1). The anomalies have an approximately decadal period. SA go on to correlate the propagating SST signals with signals in sea-level pressure. Hansen and Bezdek (1996) find similar propagating signals using a somewhat different analytical technique.

2.2. Modeling studies

Modeling and theoretical studies have identified several potential causes for decadal variability in the structure of the subtropical gyre, the Gulf Stream position and transport and the southern recirculation gyre. These causes include wind forcing, thermohaline effects and combinations of the two. Some studies find that the coupling between the two fluids is only one way, with the ocean merely responding to atmospheric anomalies. With respect to surface wind stress forcing, Frankignoul, Muller, and Zorita (1997) show that the ocean can redden the white noise spectrum of the atmosphere to generate internal decadal periods. Similarly, Sturges and Hong (1995) using empirical arguments identify westward propagating planetary waves as the cause of decadal signals in sea level at the latitude of Bermuda. As in Frankignoul et al. (1997), feed back to the atmosphere is not required for the oceanic signals.

In other studies, the two fluids are coupled and continuous interaction maintains the periodic signals. Groetzner, Latif, and Barnett (1998) argue that a quasi-decadal mode of air–sea variability simulated in their coupled General Circulation Model (GCM) involves oceanic planetary wave propagation, subtropical gyre adjustment to the waves, mean ocean currents and mean and anomalous SST distributions. The atmosphere responds to the SST anomalies and this response causes anomalies in the subtropical gyre (i.e., a $v' * T$-bar mechanism, frequently called a gyre adjustment process). The steady-state gyre response to the atmospheric forcing is delayed, as it requires propagation of planetary waves to establish.

Additionally, in the simulated eastern Atlantic, SST anomalies are caused by surface heat flux variability. These anomalies are advected westward by the mean currents (i.e., a v-bar $* T'$ mechanism). Groetzner et al. (1998) cannot determine which of the two-mechanisms is responsible for the switching of phases in the decadal mode. Both processes have similar time-scales and inadequate model data were saved to perform budget studies. The combination of these features is the cause of coupled quasi-decadal signals (17-year period) in both the intensity of the subtropical gyre, the associated SST fields of the North Atlantic and the sea-level pressure. Ezer (1999) found similar results and mechanisms in another numerical model.

Watanabe, Kimoto, Nitta, and Kachi (1999) find that gyre adjustment is the primary oceanic component of a coupled mode of decadal variability in a somewhat different GCM. However, using observations in both an EOF analysis of the upper 100 m temperature structure and a heat budget analysis of the same layer, they find that the gyre adjustment mechanism is not important for the generation and propagation of SST anomalies in the western subtropical Atlantic. Rather, eastward propagation of SST anomalies by the mean currents is found to be the dominant mechanism in the upper layers and responsible for the phase shifts at the decadal time-scales. They go on to find that gyre adjustment is responsible for observed current anomalies below 100 m (i.e., in this portion of the water column westward advection of temperature signals is prevalent). Watanabe et al. (1999) argue that in the model the upper and lower ocean layers are coupled such that gyre adjustment is responsible for the decadal signal throughout the upper ocean water column. However, in the observed ocean, the upper and lower ocean are decoupled and the v-bar $* T'$ mechanism and associated atmospheric anomalies are responsible for the decadal mode of variability.

Alternatively, surface flux forcing and thermohaline effects have been implicated in causing Gulf Stream, subtropical gyre and recirculation gyre variability. In analytical models, Cushman-Roisin (1987) and Huang (1990) attributed variability in the recirculation gyre of the Gulf Stream to surface flux forcing. Häkkinen (2000) found in a modeling and observational study that surface heat fluxes through their connection to the thermohaline circulation can lead to a decadal mode of coupled variability that includes the

basin-scale subtropical gyre. Similarly, Eden and Jung (2001) found that forcing by surface heat fluxes associated with the NAO governs the North Atlantic circulation in another numerical ocean model. Marshall, Johnson, and Goodman (2001) using simpler models than GCM's argued that both thermohaline and wind stress variability play a role in generating decadal signals. Thus, their model also includes planetary wave propagation as one component of a coupled air–sea mode of variability.

Finally, Spall (1996a, 1996b) and Meacham (2000) generated models that simulated decadal anomalies in the inertial recirculation gyres associated with the Gulf Stream. Specifically, Spall (1996a, 1996b) found that not only can the size of the recirculation gyre change on decadal time-scales, but also that these gyre changes are coincident with changes in the transport and position of the Gulf Stream. These changes are induced by interactions between the DWBC and the Stream and are independent of variability in the surface wind field.

2.3. Summary

In summary, previous observational studies have described decadal signals in Gulf Stream transport and position, sea level at Bermuda (a measure of the intensity of the subtropical gyre), the size of a recirculation gyre south of the Gulf Stream, and propagating SST signals along the path of the Gulf Stream/North Atlantic Current. Variability in any of these features can cause SST anomalies and thus potentially drive atmospheric signals. Similarly, in the atmosphere, decadal signals have been observed in the wind fields and surface heat fluxes associated with the NAO that may drive and/or be coupled to the oceanic signals. However, it should be noted that the majority of the previous observational studies only provided correlations between the ocean and atmospheric properties and used heuristic arguments to explain these relationships.

Modeling studies have offered a wide variety of mechanisms to explain the observed signals and whether they represent coupled or uncoupled modes of variability. However, in spite of the earlier observational and modeling efforts, the forcing mechanisms for the mid-latitude, decadal oceanic anomalies and the extent of the coupling of these anomalies to atmospheric variability are still open questions. Herein, observations from the western subtropical Atlantic and results from modeling efforts are used to describe further upper layer variability at annual and decadal. Particular attention will be directed at characterizing the spatial-temporal characteristics of the recirculation gyre south of the Gulf Stream and it's potential role in causing SST variability.

3. Evolution of the methodology to sample upper ocean temperature properties

Both mechanical and expendable bathythermograph (MBT and XBT, respectively) data are used in this study. MBT data are available from World War II to the mid-1960s when XBT's were introduced into oceanography. Depending on ship speed and sea state, MBT's can provide vertical profiles to 200–250 m. Initial XBT's sampled to 450 m. In the early 1970s, 750 m XBT's were introduced.

Immediately after WW II, MBT coverage in the Atlantic was primarily limited to the vicinity of the Gulf Stream as it separated from the US coast. The majority of the data were collected during academic and military research cruises with limited repeat occupations of the same section. Fig. 2 shows MBT coverage north of 20° N during two representative years.

Similarly, early applications of XBT sampling were directed primarily at basic research and military missions. Thus, as with MBT's, initial sampling was concentrated in regions of interest to these communities such as the western boundary currents of the northern hemisphere (Fig. 2). Few repeat transects were occupied in the 1960s and 1970s.

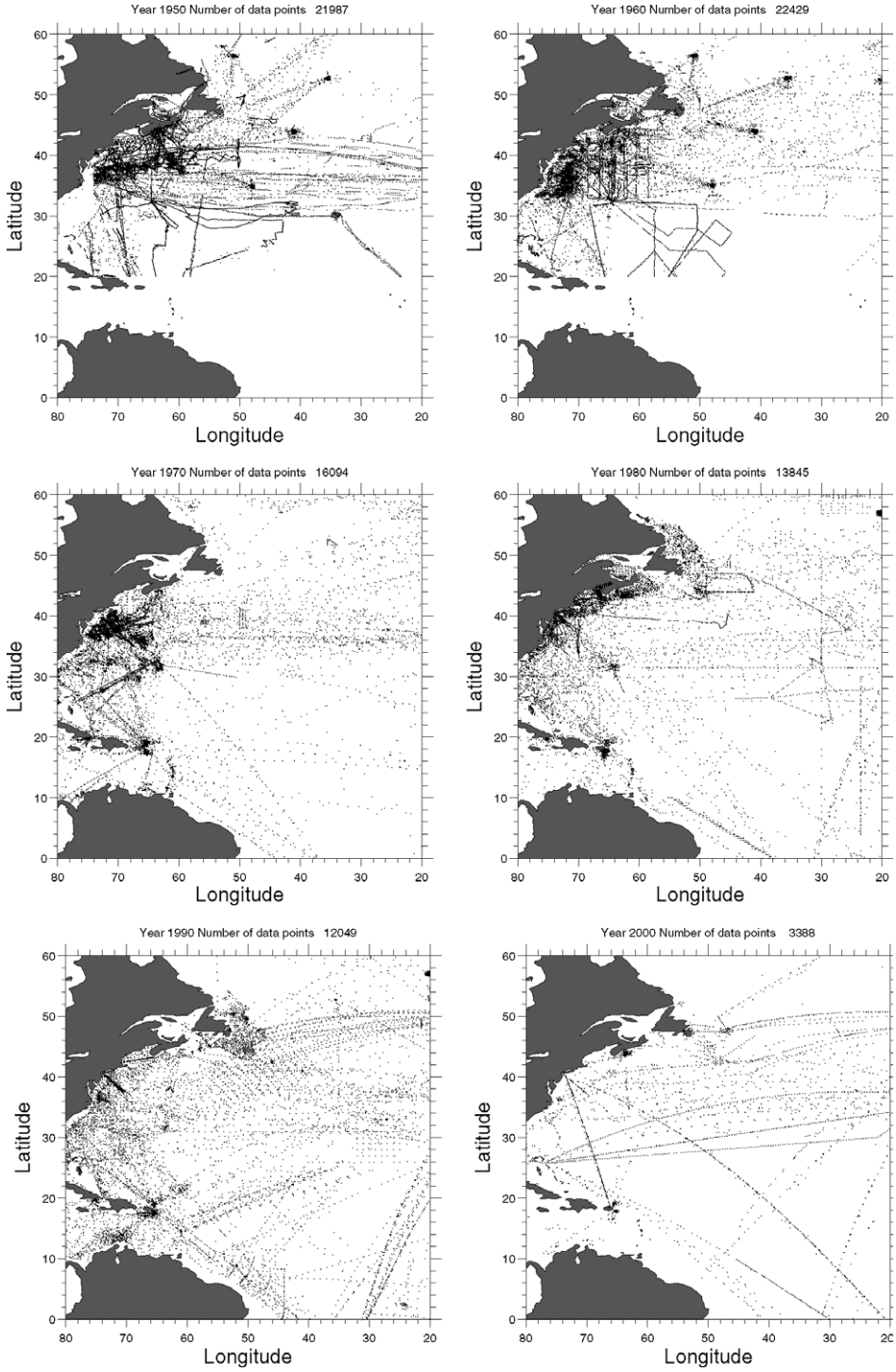

Fig. 2. Annual MBT (1950, 1960) and XBT (1970, 1980, 1990 and 2000) coverage for the years indicated. Only MBT data north of 20° N were retrieved for this study.

As the role of the ocean in such coupled climate phenomena as ENSO became evident, the need for sustained and repeat observations was realized. New sampling strategies that employed Voluntary Observing Ships (VOS), primarily commercial vessels, were developed. Both the Tropical Ocean Global Atmosphere (TOGA) and World Ocean Circulation Experiment (WOCE) were responsible for the institution of regularly re-occupied VOS transects.

Three types of line sampling were developed during TOGA and WOCE. Fig. 3 shows the TOGA/WOCE distribution of all the types of VOS transects in the Atlantic Ocean. XBT's along Low Density, LD, transects are deployed by ship's personnel at a desired rate of four probes per day. Spatial resolution is thus a function of ships' speed. Typical merchant ship speeds range from 7 to 12 m/s resulting in station spacing of 150–250 km. Desired temporal resolution is monthly. However, because of the vagaries of VOS routing (i.e., ships' frequently change routes), this resolution is often difficult to obtain. These sampling requirements are based on objective analyses of historical surface and subsurface temperature data (e.g., Sprintall & Meyers, 1991; Meyers, Phillips, Smith, & Sprintall, 1991; Festa & Molinari, 1992; White, 1995).

High Density, HD, lines were initiated to provide increased spatial resolution along select transects (see the figure legend for Fig. 3 for location of HD lines). Station spacing is eddy resolving with typical XBT separation of 50 km in the ocean interior, decreasing close to ocean boundaries and across major current systems. Desired temporal resolution is seasonal. The HD lines presently require technical support to ride the VOS and collect the data. Frequently repeated lines, FR, lines are located in regions of large temporal variability such as the tropics (see the figure legend for Fig. 3 for location of FR lines). Spatial sampling is

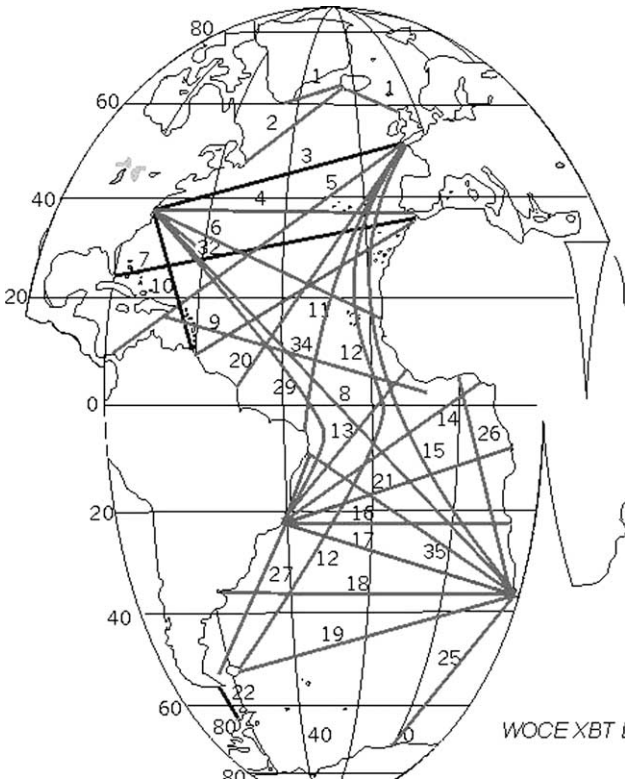

Fig. 3. WOCE/TOGA XBT transects in the Atlantic. High density lines include 7, 8, 10, 11 and 18. Frequently sampled transects include 8, 11 and 20. All other lines are occupied in low density. See text for description of sampling.

the same as LD but temporal sampling is 18 times per year. Fig. 2 demonstrates the transition with time from primarily research cruise coverage in the 1960s and 1970s to primarily repeat transect coverage in the 1990s.

The resulting XBT and MBT data can be used in at least two ways. Firstly, the data from many lines and research cruises can be averaged in time and mapped onto spatial grids to provide two-dimensional representations of upper layer temperature structure and it's evolution. The spacing of recent lines (Fig. 2) necessitates rather coarse resolution for mapping.

Secondly, some lines have been occupied for many decades and through generation of time–distance plots the resulting data can be used to provide increased details of the evolution of the upper layer temperature field. Herein, we use both approaches to study decadal variability of the transport and position of the Gulf Stream and the shallow recirculation gyre described by WK. We have selected A-10 as the primary transect for study because of data availability and the path, which crosses the Gulf Stream and subtropical gyre (Fig. 4). Until recently A-10 was occupied as a LD line, but over the past several years it has also been occupied as a HD line.

In addition to XBT lines, future temperature and salinity sampling networks will also include profiling floats (see Davis, Webb, Regier, & Dufour, 1992; for a description of the floats). The Atlantic Climate and Circulation Experiment (ACCE) represented the last field phase of WOCE and began in 1997. Deployment of a profiling float array in the North Atlantic was one component of ACCE (see Table 1 for data sources). The ACCE floats typically provided temperature profiles to a depth of 1000 m every 10 days. Fig. 5 shows profile locations for the years 1998–2001. The float and XBT representations of the shallow recirculation gyre are compared to demonstrate the capabilities of the float system as a long-term monitoring tool.

4. Data sources and analyses

Sources and temporal characteristics of all the data used in this study are listed in Table 1. The 1990–1998 XBT data were quality controlled using procedures outlined in Daneshzadeh, Festa, and Minton (1994). Both types of BT data were also quality controlled during mapping onto time–distance plots, ver-

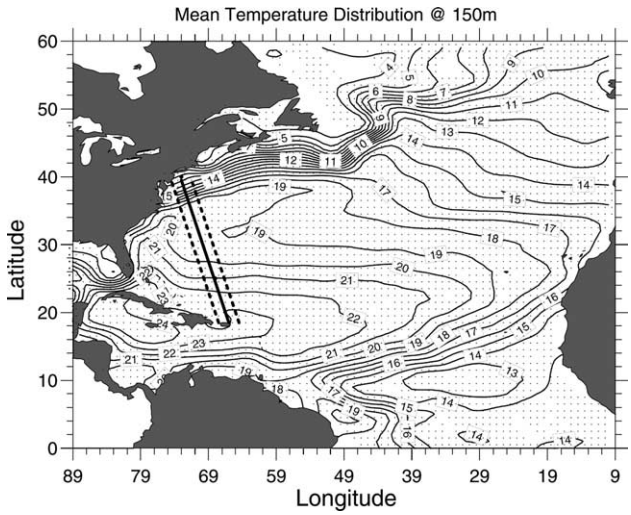

Fig. 4. The mean annual distribution of temperature (°C) at 150 m. The 3-degree swath enclosing the A-10 sections is shown. The rms difference between raw and gridded temperature computed over the entire horizontal domain by the mapping routine is 0.42 °C.

Table 1
Data sources and record lengths (T/P = Topex/Poseidon)

Data type	Source	Record length
Mechanical	www.nodc.noaa.gov/	1960–1966
Bathythermographs	OC5/pr_wodv2.html	
Expendable Bathythermographs	www.aoml.noaa.gov	1967–2003
Profiling floats	WOCE Data Products Committee (2002)	1998–2001
NAO index	Hurrell (1995)	1865–2000
Gulf Stream position from		
(a) Subsurface temperature data	Joyce et al. (2000)	1955–1998
(b) SST data	Taylor and Stephens (1998)	1966–1988
(c) Subsurface temperature data	This study	1950–2003
Gulf Stream transport from		
(a) Hydrography	Sato and Rossby (1995)	1932–1988
(b) Hydrography	Curry and McCartney (2001)	1954–1997
(c) XBT and climatological salinity data	This study	1967–2003
(d) Direct velocity observations	Halkin and Rossby (1985)	1980–1983
(e) Geosat altimetry data	Kelly (1991)	1986–1989
Florida Current transport	Baringer and Larsen (2001)	1982–2002
Size of shallow recirculation gyre	Wang and Koblinsky (1996)	
(a) T/P data		1993–1994
(b) Geosat data		1987–1988

tical sections or horizontal depth surfaces. Variable values that were two standard deviations from the mean grid point value (typically on the order of 5%) were not used in the analyses.

4.1. Gulf stream position

The near surface core of the Gulf Stream on the A-10 section is taken as the latitude of the 15 °C isotherm at 150 m (Fig. 4). A depth shallower than the 200 m used by JDS, was selected to maximize the inclusion of MBT data in the calculations. However, as observed in Fig. 6 for the mean temperature section, there is little difference between the position of the 15 °C at 150 and 200 m (as is the case for the synoptic sections, not shown). Combining the two data sets resulted in a time-series extending from 1949 to 2003.

A time–latitude plot of temperature at 150 m was generated from BT's collected within ±1.5° of the nominal location of A-10 (Fig. 4) for a shortened version of the transect, 32–40° N. Because of limitations in the mapping software, the shorter section was needed for 22 km grid spacing. Temporal resolution was monthly. To distinguish between individual monthly values and mean monthly values, the term year–month will be used for the former.

The routine used for mapping the data onto vertical sections and horizontal surfaces is modified from Wabba and Wendelberger (1980). This method does not use structure or correlation functions for the mapping as in other objective mapping methodologies but ''may be thought of as a very general form of low-pass filter'', Wabba and Wendelberger (1980). Error fields that can be generated when using the structure or autocorrelation functions are not available in this method. However, an overall index for uncertainty is provided by the standard deviation (rms) of the difference between the observed and gridded values. These values will be given on the figure legends for the plots of vertical sections and horizontal distributions.

The latitude of the 15 °C isotherm on the 150 m surface was estimated from the year–month time–latitude plots by linear interpolation between adjacent grid points. Mean monthly Stream positions were then calculated from the year–month record. Mean monthly standard deviations within the quadrangles in the axis of the Stream at 150 m were greater than 1.5 °C, consistent with the large horizontal gradients in this

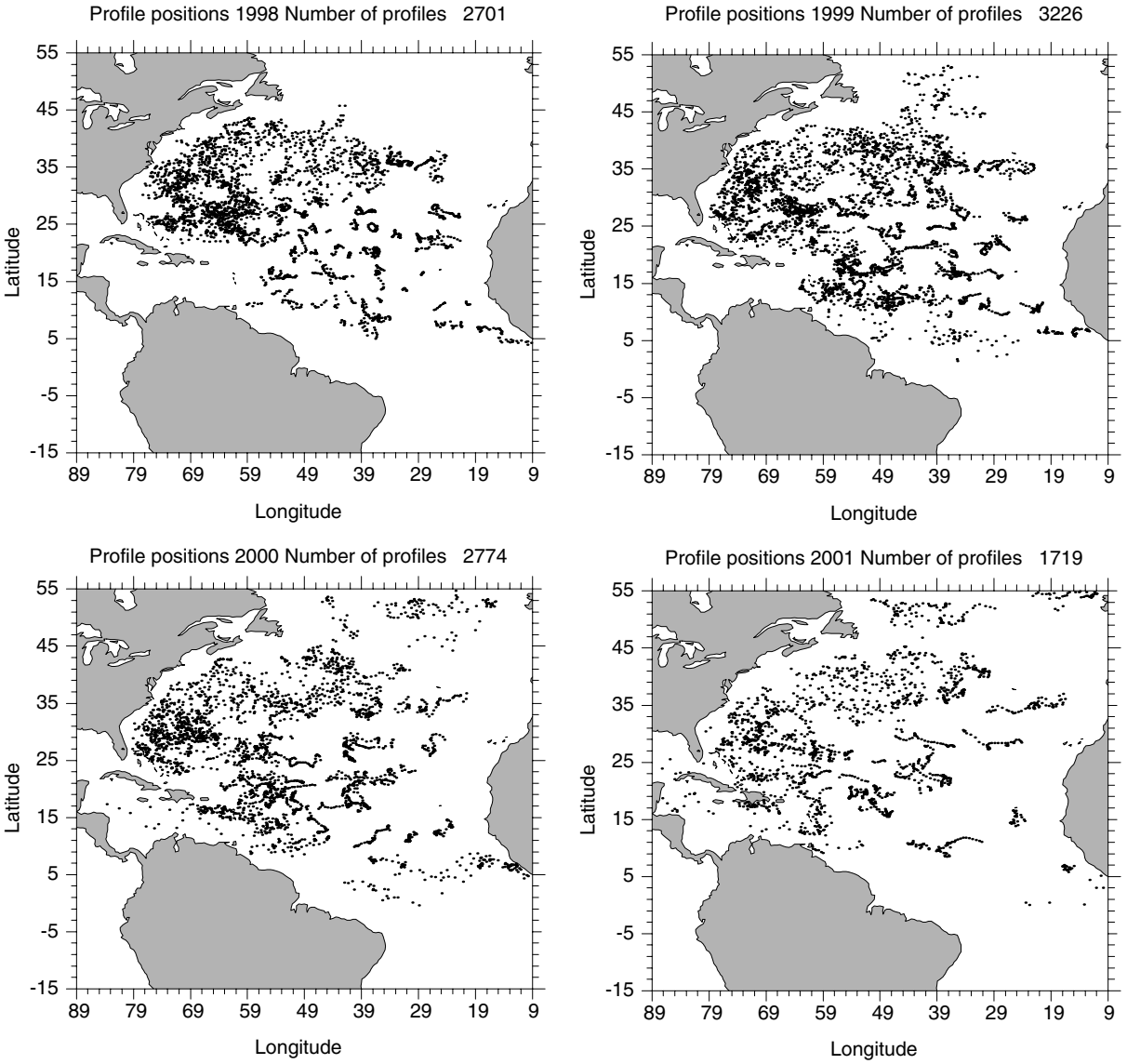

Fig. 5. Location of temperature profiles by year derived from profiling floats deployed during the Atlantic Climate and Circulation Experiment.

region (shown in Fig. 6 for the mean annual A-10 temperature section). The year–month standard deviations in the area of the axis were about 3 °C. A qualitative propagation of error analysis was performed to determine uncertainties in the axis location. It was assumed that the majority of the error in estimating the position of the core is in the uncertainty in the temperature observations rather than in the positions of the data points within a quadrangle (i.e., a large number of points at some distance from the center of the quadrangle would introduce an error in the distance used in the linear interpolation). An uncertainty in the mean monthly (year–month) positions of the core of about 20 (30) km is estimated.

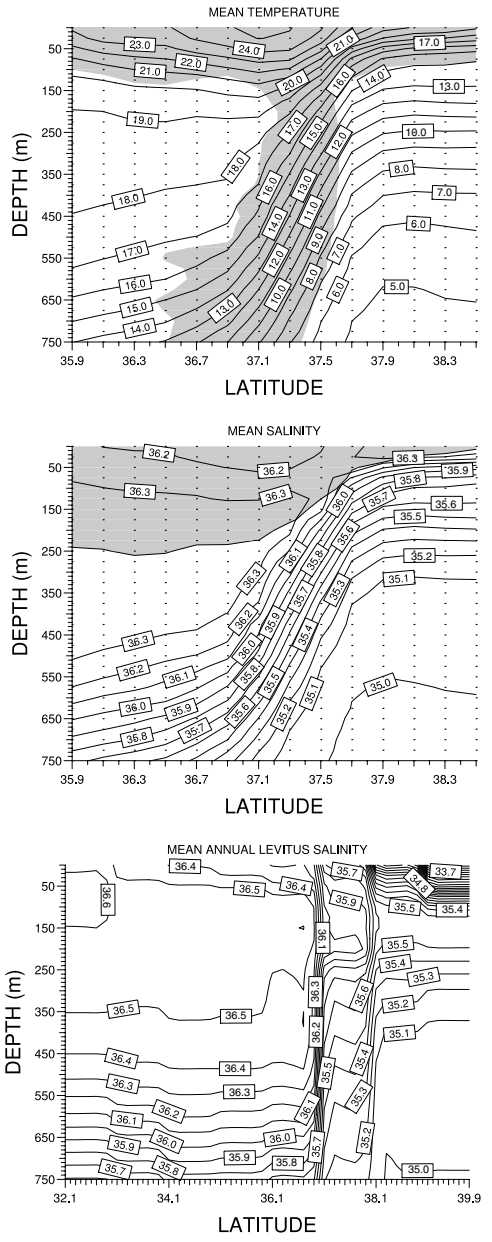

Fig. 6. Upper panel: Mean annual vertical temperature (°C) section along A-10. Shaded areas encompass standard deviations of temperature greater than 1.5 °C. The rms difference between raw and gridded temperature computed over the entire section by the mapping routine is 0.07 °C. Middle panel: Salinity section derived from the temperature section of the upper panel and the temperature–salinity relationship of area 11 from Emery and Dewar (1982). Shaded areas encompass standard deviations of salinity greater than 0.1. The rms difference between raw and gridded salinity computed over the entire section by the mapping routine is 0.04. Lower panel: Salinity section derived from the temperature section of the upper panel and the temperature–salinity relations from the climatology of Conkright et al. (2002). The rms difference between raw and gridded salinity computed over the entire section by the mapping routine is 0.02. For all the panels, horizontal spatial resolution is 22 km along A-10 and vertical resolution is 25 m to 400 m. Grid points with data are indicated by dots.

4.2. Gulf stream transport

Geostrophic transports through A-10 are computed relative to three reference levels, 300, 450 and 750 m. Mean and mean monthly transports are estimated for the 300 and 750 m reference levels. A time series of mean annual transports from 1967 to 2003 was computed for the 450 m level. Similar procedures were used in the three transport calculations. First, year–month temperature sections were computed using all profiles collected within a 4-degree swath of the mean position of the shortened version of A-10 for each month from 1967. The larger swath than used in the computations of the position of the Gulf Stream axis was required to ensure that sufficient deeper data were available for the geostrophic calculations.

The year–month temperature sections were then re-gridded from the geographical reference frame to one using the latitude of the 15 °C isotherm at 150 m as the zero coordinate (i.e., the position of the core of the Gulf Stream is taken as the reference point). The re-referencing greatly reduced the amount of data available to estimate temperature sections as compared to doing a Eulerian average, which would employ all available data (i.e., only sections that crossed the axis of the Stream could be used). However, this procedure resulted in more accurate representations of the temperature transects by preserving gradients. Mean monthly temperature sections were then computed from the year–month time series.

Several options are available to estimate salinity for computation of density, dynamic height and then geostrophic velocities and transports. Conkright et al. (2002) provide monthly averages of salinities above 1000 m on a one-degree by one-degree grid. As noted by Lozier, Owens, and Curry (1995), for example, combining depth averaged salinity (e.g., from Conkright et al., 2002) with depth-averaged temperatures (e.g., estimated for A-10) does not preserve the observed temperature–salinity relationships and can adversely affect geostrophic calculations. Thus, to compute dynamic heights, the mean monthly temperature data were matched to salinity data from the temperature–salinity relationships given in Emery and Dewar (1982).

The A-10 transect crosses two of Emery and Dewar's (1982) salinity regions, 11 and 12. The boundary between the 5° by 5° quadrangles crossed by A-10 is located at 35° W, some 2° to the south of the mean axis of the Stream, Fig. 4. Thus, area 12 includes the axis of the Stream and the shelf waters to the north of the core resulting in larger standard deviations around the mean temperature–salinity relation than estimated for area 11.

A salinity section developed from the mean temperature section of Fig. 6 and the temperature–salinity relation of region 11 from Emery and Dewar (1982) is given in Fig. 6. Another salinity section was constructed from the mean temperature section and the salinity values from the climatology of Conkright et al. (2002). Particularly in the region equatorward of the axis of the Stream, the salinities from region 11 are close to those of Conkright et al. (2002), Fig. 6. The salinities from region 12 (not shown) are some 0.3–0.4 lower than those given in the climatology in this area.

The surface layer to the north of the Stream is a region of large differences in region 11 and 12 salinities. Here, the lower salinities associated with region 12 are similar to the climatological values of Conkright et al. (2002), while those from region 11 are higher. However, the salinity differences are limited to depths shallower than 100 m and have only a small effect on the total transport estimates (less than 2 Sv). Thus, salinities from region 11 appear more representative of average conditions within and to the south of the core and are used in all geostrophic calculations.

Geostrophic velocities were estimated as a function of depth relative to the three reference levels between each grid point. For the mean and mean monthly transports relative to 300 and 750 m, the width of the Stream was taken to extend between the negative velocity values bounding the core. The average width at both depths using this definition was 176 km. The 450 m mean annual transports were computed from the nine grid points, 200 km, surrounding the core of the Gulf Stream. The different definition of the Stream width was necessary since several mean annual sections do not extend to the edges of the Stream as defined for the 300 and 750 m levels because of the paucity of data on this time-scale.

4.3. Recirculation gyre

The recirculation gyre of WK is a shallow feature extending down to the level at which the annual cycle becomes small, typically about 250–300 m south of the Gulf Stream. The northeastern extension of the gyre generated from an EOF analysis of the altimetry data is approximately coincident with a perturbation in the shape of the 15 °C isotherm at 150 m that moves seasonally (Fig. 7). The location of this perturbation will be used as an index for the mean monthly size of the WK gyre.

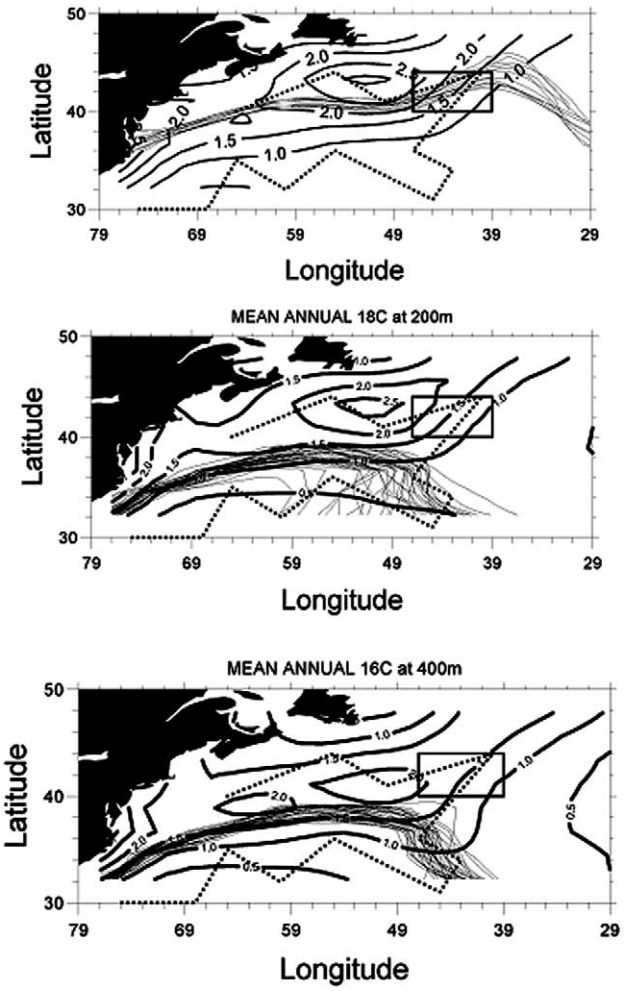

Fig. 7. Upper panel: Mean monthly contours of the 15 °C isotherm at 150 m, light lines. Standard deviation (°C) of the temperature field at 150 m, thick lines. The average monthly rms difference between raw and gridded 150 m temperature distributions computed by the mapping routine is 1.1 °C. The rms difference between raw and gridded standard deviation values is 0.4 °C. Middle panel: Mean annual contours of the 18 °C at 200 m for the years 1967–2003. The average annual rms difference between raw and gridded 200 m temperature distributions computed by the mapping routine is 1.1 °C. The rms difference between raw and gridded standard deviation values is 0.1 °C. Lower panel: Same as middle panel, except for 16 °C at 400 m. The average monthly rms difference between raw and gridded 400 m temperature distributions computed by the mapping routine is 1.1 °C. The rms difference between raw and gridded standard deviation values is 0.1 °C. All panels: The Wang and Koblinsky (1996) gyre from Fig. 1, dotted lines and area C from Curry and McCartney (2001), see Fig. 1 and text for details. Data are gridded onto a 2° of latitude by 2° of longitude grid.

The CM results suggest that at time-scales longer than annual, variability in the size of the southern recirculation gyre extends through the main thermocline. Thus, to study the decadal signal in gyre size and have sufficient XBT data to map the temperature fields, temperature distributions at 200 and 400 m were used. Specifically, the 18 °C isotherm at 200 m and 16 °C isotherm at 400 m are located near the northeastern extension of the WK gyre (Fig. 7). The northeastern extension of these isotherms was used to define the decadal signal in gyre size.

Estimates of uncertainty in the size of the gyre at 150, 200 and 400 m are calculated using the same qualitative propagation of error analysis used to define uncertainties in the position of the Gulf Stream. To determine the size of the gyre, temperature data at these depths were mapped onto a 2° of latitude by 2° of longitude grid first by year–month and then by month and year. At this depth, the eastern extensions of the mean monthly 15 °C isotherm at 150 m and the mean annual extensions of the 18 °C at 200 m and the 16 °C isotherm at 400 m are located in a region where the standard deviation of temperature is of the order 1 °C (Fig. 7). Using this standard deviation in the error analysis, results in an uncertainty in the eastern extension of the southern recirculation gyre at the three depths and on mean monthly and interannual time-scales of 240 km.

4.4. Atmospheric variability

The NAO has been correlated with various oceanographic signals in the North Atlantic (e.g., CM and JDS) and is thus taken as a measure of atmospheric variability that may be coupled to oceanic anomalies. Specifically, the NAO index of Hurrell (1995), extended to the year 2000, is used for this purpose.

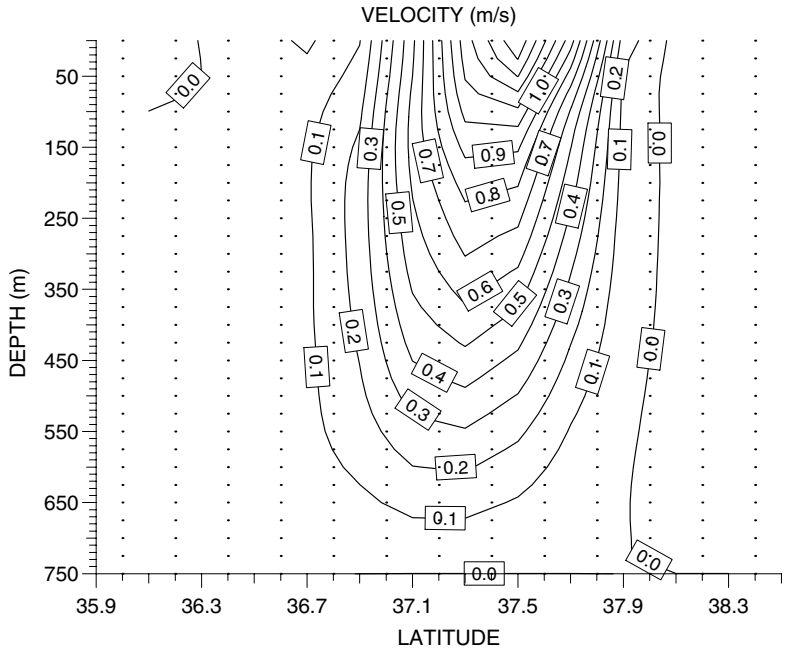

Fig. 8. Mean annual A-10 geostrophic velocity (m/s) section computed relative to a reference level at 750 m (see Fig. 1 for A-10 location) using the mean temperature and salinity (middle panel) sections shown in Fig. 6. Grid points with data are indicated by dots. The rms difference between raw and gridded velocity computed over the entire section by the mapping routine is 0.03 m/s. See text for method of preparing section.

To highlight decadal signals, year–month time-series of the NAO, Gulf Stream position and transport from A-10 and easternmost extension of the southern recirculation gyre of the Stream were generated. Monthly anomaly series were then estimated by subtracting mean monthly values of each variable. A time-series of annual anomaly values was then generated and smoothed with a three-year running boxcar average. The common time-period for all the time series is 1968–1997 (Table 1).

5. Results

In this section, a discussion of the average properties of temperature, salinity, velocity and transport along A-10 is provided first. The annual cycles of these properties, Gulf Stream transport and position, and the size of the WK recirculation gyre are then described, followed by a description of the decadal signals in these features. The final subsection will consider the sampling implications of the three previous subsections. Throughout, uncertainty estimates for the variables being described are given.

5.1. Average vertical sections and gulf stream transports

The average temperature section and an indication of temperature variability along A-10 are given in Fig. 6. Several characteristics of the temperature structure of the western subtropical Atlantic are apparent. The intense horizontal temperature gradients indicative of the Gulf Stream appear between 36° N and 38° N at this longitude (~72° W, Fig. 4). South of the Gulf Stream, the reduced vertical temperature gradients

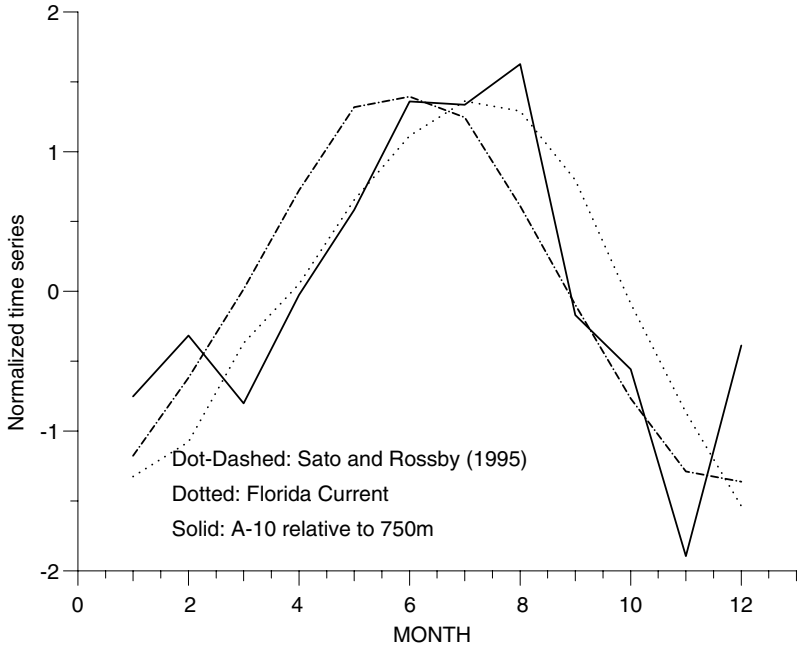

Fig. 9. Normalized by record length standard deviation, SD, mean monthly transports of (1) Gulf Stream transport at A-10 computed relative to 750 m and smoothed with a 3-month box car filter, SD = 1.37; (2) Florida Current transport at 27° N smoothed with a 3-month box car filter, SD = 0.94; and (3) Gulf Stream transport relative to 2000 m from Sato and Rossby (1995) fit with an annual cycle, SD = 2.69.

associated with 18 °C Water are centered at about 350 m. The main thermocline is located below the 18 °C Water. The warm core of the Gulf Stream is characterized by a dip in the isotherms just south of the Stream. This core results in a "negative thermal wind shear on the offshore side of the current" and a corresponding subsurface velocity core (Johns, Shay, Bane, & Watts, 1995).

Standard deviations of the mean annual temperature field are largest both near the surface and coincident with the axis of the Gulf Stream. The large near surface standard deviations are related to the annual cycle in surface temperatures. At depth, the large values coincident with the Stream axis are related, in part, to meridional translations of the core, as will be described. The mean annual salinity section derived from the temperature–salinity relation from region 11 of Emery and Dewar (1982) is also given in Fig. 6. Largest standard deviations associated with the mean salinity field are near the surface.

The geostrophic velocity section derived from the portion of the 750 m temperature transect that includes the core of the Stream is given in Fig. 8. The maximum surface velocity on the section is more than 1.3 m/s (the 1.4 m/s contour is an artifact of the contouring routine). There is a slight southward shift of the current axis with depth located to the south of the core as observed in earlier studies (e.g., Halkin & Rossby, 1985; HR, Johns et al., 1995).

Confidence in the A-10 velocity section can be obtained through comparison with earlier work. HR described data from 16 transects crossing the Gulf Stream at about 73° W, closely paralleling A-10. Measurements consisted of direct velocity observations that extended to the sea floor. The HR mean velocity section has surface speeds greater than 1.5 m/s. The speed in the core of the average HR section at 750 m is 0.4 m/s (their Fig. 10). The maximum mean geostrophic speed along A-10 of 1.3 m/s relative to 750 m (Fig. 8) is

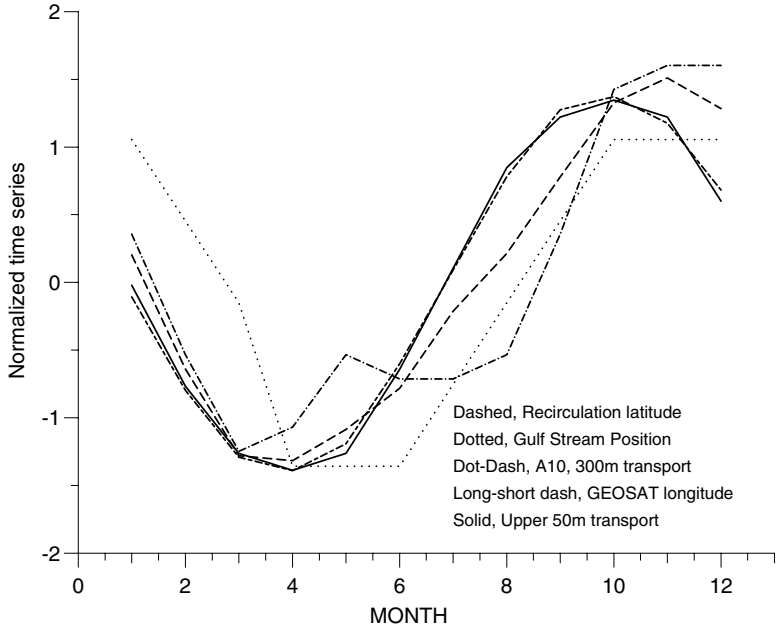

Fig. 10. Normalized by record length standard deviation, SD, mean monthly (1) easternmost location of the 15 °C isotherm at 150 m, smoothed with a 3-month box car filter, SD = 1.08; (2) residual sea surface height anomalies of the first EOF representing a shallow recirculation gyre south of the Gulf Stream from Geosat data (Wang and Koblinsky, 1996), SD = 1.01; (3) A-10 geostrophic transports computed relative to 300 m and smoothed with a 3 month box car filter, SD = 0.19; (4) transport of the upper 50 m derived from altimetric dynamic height differences across the Stream from Kelly (1991), see text for explanation, SD = 0.40; and (5) A-10 Gulf Stream position, SD = 0.06.

Table 2
Mean and range of annual and decadal signals from selected time series and uncertainty estimates

Variable	Source	Annual signal (mean/range/uncertainty)	Decadal signal (mean/range/uncertainty)
Florida Current Transport[a]	Baringer and Larsen (2002)	32.0/2.7/1 Sv[d]	N.A.
Gulf Stream transport >A-10			
Relative to 300 m[a]	This paper	5.5/1.0/1.6 Sv	N.A.
Relative to 450 m[a,c]	This paper		12.2/0.8/0.9Sv
Relative to 750 m[a]	This paper	36.1/4.9/3.4 Sv	N.A.
>73° W	Sato and Rossby (1995)		
Relative to 2000 m[b]		71.4/7.4/8.0 Sv	N.A.
Relative to 2000 m	Curry and McCartney (2001)	N.A.	60.0/10.6/5.0 Sv
Upper 50 m transport from altimetry[b,e]	Kelly (1991)	6.9/1.1/1.3Sv	N.A
Gulf Stream position >A-10[a,c]	This paper	36.7° N/14/20 km	36.7° N/43/30 km
>	Joyce et al. (2000) N.A.	N.A./100km/N.A.	
Shallow recirculation gyre size[a,c]			
Monthly @ 150 m	This paper	43.6° W/650/240 km	N.A.
Annual @ 200 m	This paper	N.A.	51.3° W/500/240 km
Annual @ 400 m	This paper	N.A.	46.2° W/140/240 km

See Table 1 for record lengths, Fig. 1 for data locations and the text for methods of computing uncertainties. N.A. = not available.
[a] Monthly mean values smoothed with a 3-month boxcar filter.
[b] Monthly mean values fit with an annual cycle.
[c] Annual mean values smoothed with a 3-year boxcar filter. Range taken as average of difference between post-1970 extremes.
[d] Baringer (2004) personal communication.
[e] Based on 0.2 m/s uncertainty in Geosat surface velocity estimates.

similar to the HR surface speed relative to 750 m of 1.1 m/s, particularly in view of the different times and observing techniques used for each estimate.

The geostrophic transport of the Gulf Stream computed from the velocity section in Fig. 8 is 36.1 Sv. Uncertainties in this estimate can be introduced by uncertainties in the salinity and temperature observations used in the computation of density. Geostrophic transport calculated by adding (subtracting) one standard deviation of temperature at each grid point is 38.6 (35.7) Sv and by adding (subtracting) one standard deviation of salinity is 35.2 (37.0) Sv. The differences in transport caused by the uncertainties in the temperature (2.9 Sv) and salinity (1.8 Sv) estimates provide a measure of uncertainty in the total transport, 3.4 Sv.

Hogg (1992), using the direct velocity observations of HR, estimated a mean annual baroclinic transport relative to 1000 m at 73° W of 47.4 Sv. Fig. 10 in HR has a mean velocity of about 0.18 m/s between 750 and 1000 m within the Stream (width of 180 km) resulting in a transport is this portion of the water column of 8.3 Sv. Subtracting 8.3 Sv from Hogg's (1992) 1000 m transport results in a baroclinic transport between the surface and 750 m at the HR section of 39.1 Sv. Thus, the Hogg (1992) transport estimate is within the uncertainty limits of the A-10 value (36.1 ± 3.4 Sv).

5.2. Annual cycles

Fig. 9 includes normalized mean monthly geostrophic transports of the Gulf Stream relative to 750 m at A-10. Uncertainties in these values are computed by first estimating transport from temperature and salinity values plus and minus one standard deviation from the mean (as above). Average absolute differences in mean monthly values caused by temperature (salinity) uncertainties are 2.0 (1.9) Sv. Thus, the uncertainty in the mean monthly transports is taken as 2.7 Sv. The mean error value, 3.4 Sv, is greater than this value because of larger near surface standard deviations in the mean temperature and salinity profiles transects than in the mean monthly sections.

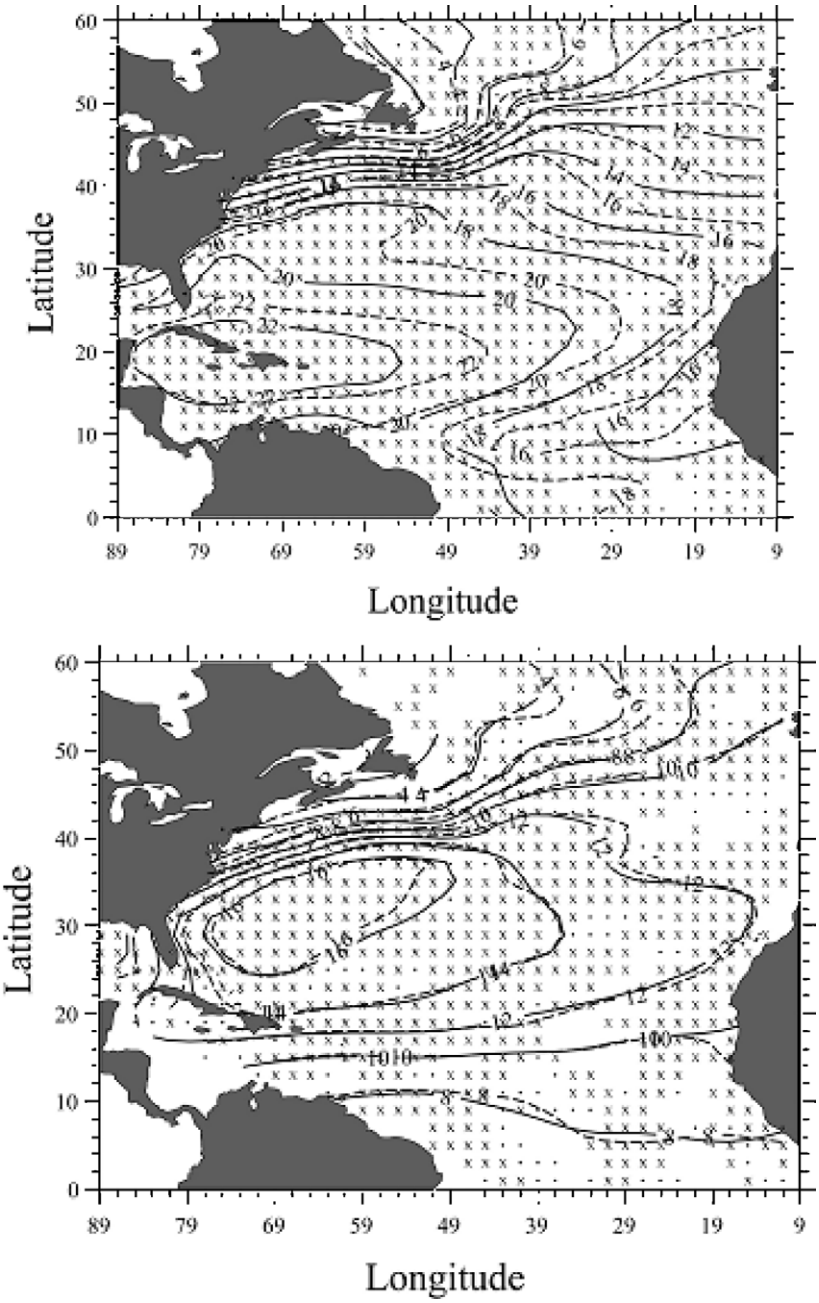

Fig. 11. Upper panel: Depth averaged temperature of the upper 300 m for the months of April and November. The rms difference between raw and gridded April (November) temperature distribution computed over the entire section by the mapping routine is 0.6 (0.6) °C. Lower panel: Depth averaged temperature of the 400–600 m layer for the months of April (dashed) and November (solid). The rms difference between raw and gridded April (November) temperature distribution computed over the entire section by the mapping routine is 0.7 (0.7) °C. The months represent minimum (April) and maximum (November) gyre size determined from the distributions of the 15 °C isotherm at 150 m (Fig. 10).

Fig. 9 provides mean monthly values of total Florida Current transport at 27° N and mean monthly values of geostrophic transport of the Gulf Stream relative to 2000 m from Sato and Rossby (1995). The Sato and Rossby (1995) transports were estimated from pairs of hydrographic stations that straddled the Gulf Stream between 66° W and 74° W. An annual cycle was fit to the raw values to arrive at the curve given in Fig. 9. An annual cycle was not fit to the other two curves. The three annual cycles are in phase to within two months, with maximum transport observed in June, July or August and minimum transport in November or December.

A different annual cycle is found when considering shallower transports. The annual cycle from A-10 of normalized transport computed relative to a 300 m reference level is shown in Fig. 10. Uncertainty in mean monthly transport relative to 300 m was calculated in the same manner as for the 750 m computations, resulting in an error estimate of 1.6 Sv. Kelly (1991), using the annual cycle of dynamic height slope across the Gulf Stream from GEOSAT, inferred the transport of the upper 50 m of the current. This annual cycle is given in Fig. 10 and the range of transport at this period is given in Table 2. Fig. 10 also shows the mean monthly positions of the core of the Gulf Stream.

The normalized mean monthly easternmost positions of the 15 °C isotherm at 150 m and the amplitude of the first EOF mode of residual sea surface height anomalies from GEOSAT taken by WK to represent the temporal evolution of the shallow gyre are given in Fig. 10. It should be noted that WK also generated a similar time-series from T/P data (not shown) that leads the GEOSAT series by several months. WK suggest that interannual variability and resolution differences between the satellites could contribute to the different phasing.

In summary, the phases of the annual cycles of the shallow Gulf Stream transport and position and gyre intrusion derived from the BT data are consistent with the WK and Kelly (1991) values derived from

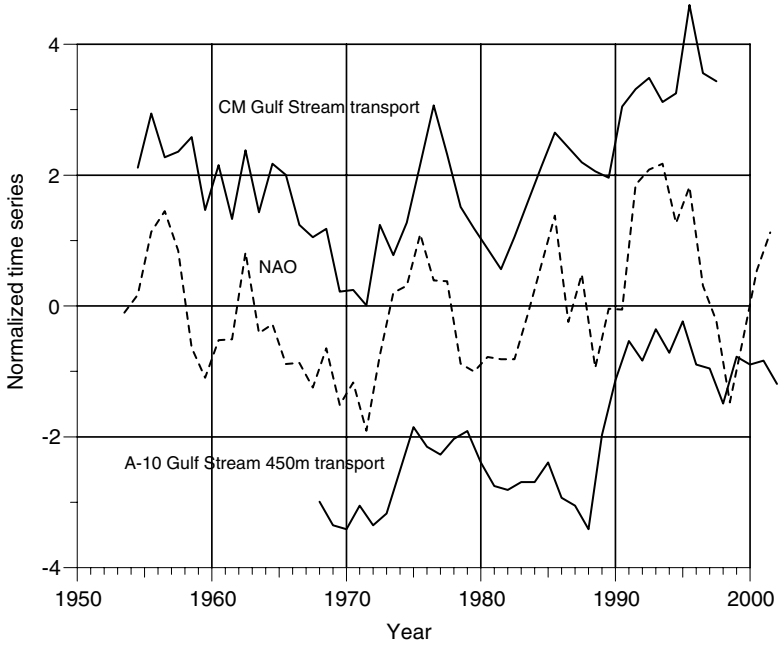

Fig. 12. Normalized by record length standard deviation, SD, time series of (1) combined Gulf Stream and North Atlantic Current geostrophic transports computed relative to 2000 m from Curry and McCartney (2001), CM transport, using the station positions shown in Fig. 1, SD = 4.84; (2) NAO index from Hurrell (1995), smoothed with a 3-year box car filter, SD = 0.44; and (3) A-10 geostrophic transport computed relative to 450 m and smoothed with a 3-year box car filter, SD = 0.56.

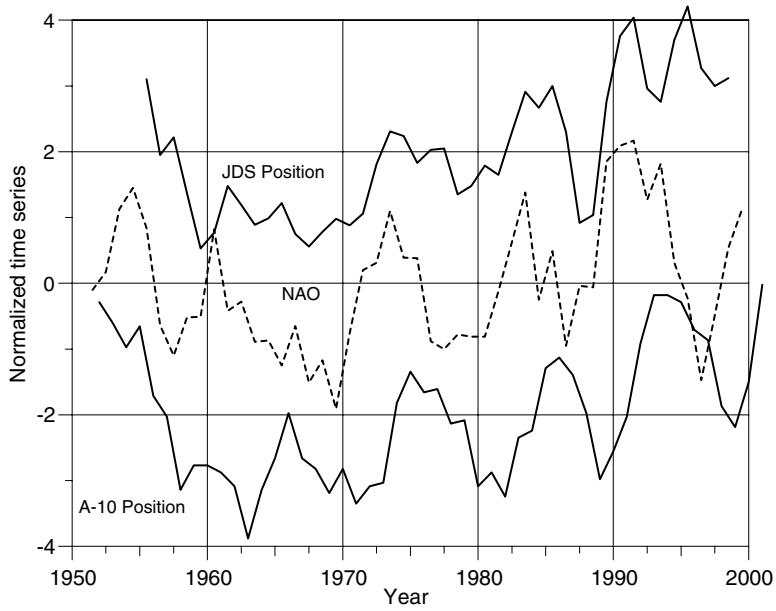

Fig. 13. Normalized by record length standard deviation, SD, time series of (1) Gulf Stream position taken as the position of the 15 °C isotherm at 200 m from the EOF analysis of Joyce et al. (2000), JDS position, SD = 1.53; (2) NAO index, smoothed with a 3-year box car filter, SD = 0.44; and (3) Gulf Stream position at A-10 taken as the position of the 15 °C isotherm at 150 m, smoothed with a 3-year box car filter, SD = 0.21.

satellite altimetry data. Specifically, these times-series exhibit maximum transport, northern Stream position and gyre intrusion in fall and minimum values in the spring (Fig. 10). However, the 300 m-transport time series are out of phase with the transports referenced to greater depths shown in Fig. 9 which have a maximum (minimum) in late spring–summer (fall).

Maximum (minimum) gyre size determined from the 15 °C isotherm at 150 m occurs in the mean monthly temperature fields in November (April) similar to the signal estimated by WK from altimetry data (Fig. 10). The distribution of the depth averaged temperature of the upper 300 m and the layer between 400 and 600 m were mapped for these two months to illustrate the depth dependence of gyre size changes (Fig. 11). The upper panel shows a large seasonal change in gyre size. The lower panel of Fig. 11 shows little change in the contours between the two months indicating that the annual cycle in gyre size is limited to depths shallower than 400 m. These depth dependent differences in temperature structure support the WK finding of a shallow character for the seasonal cycle of the recirculation gyre.

5.3. Decadal signals

The common record length of all the time series extends only from 1968 to 1997. As will become evident, during this 30-year interval, all the variables exhibit three decadal-like oscillations that are very similar in phase. Thus, correlations between various characteristics of the Gulf Stream, gyres and atmospheric properties are typically high and will not be given because of the short record length relative to the dominant period (i.e., significance is limited). However, phase lags and correlations between records with longer overlap will be discussed. The ranges of the decadal signals, computed as average of differences between extreme events in a time series after 1970, are given in Table 2.

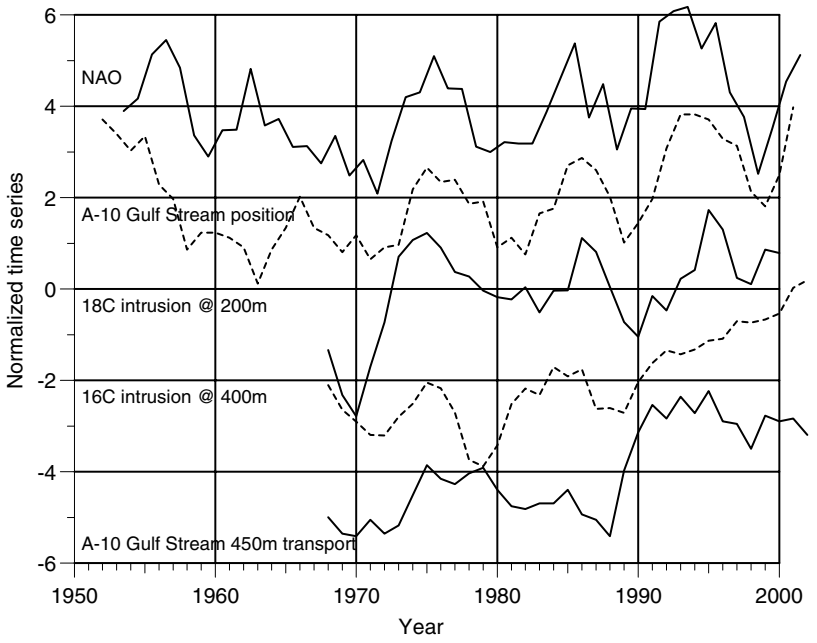

Fig. 14. Normalized by record length standard deviation, SD, time series of (1) NAO, SD = 0.44; (2) Gulf Stream position at A-10, SD = 0.21; (3) northeastern most extension of the 18 °C isotherm at 200 m, SD = 2.38; (4) northeastern most extension of the 16 °C isotherm at 400 m, SD = 1.06 and (5) Gulf Stream transport at A-10 relative to 450 m, SD = 0.56. All records were smoothed with a 3-year boxcar filter.

The time series of geostrophic transport relative to 450 m through A-10 is given in Fig. 12. Uncertainty in these transports was estimated in a similar manner to that used for the mean monthly 300 and 750 m transports. Annual transports were computed using the annual temperature (salinity) plus and minus one standard deviation of temperature (salinity) at each grid point. The average absolute transport difference between the two temperature (salinity) distributions is 0.7 (0.6) Sv. The resulting uncertainty in the annual transports is 0.9 Sv.

The CM time series of geostrophic transport relative to a 2000 db reference level and that of the A-10 geostrophic transport relative to 450 m are shown in Fig. 12. Both records include an increase in Gulf Stream transport and the occurrence of decadal-like signals after 1965–1970. In addition, the 1985 relative maximum in transport in both records is smaller than the maximum in the 1970s and 1990s.

The time series of Gulf Stream position along A-10 and from JDS are shown in Fig. 13. Both include a northward trend in Stream position and decadal-like signals after 1965–1970. The range of latitudinal movements of the non-normalized Stream position at A-10 (48 km, Table 2) is somewhat larger than the range of the annual signal (14 km, Table 2) similar to the findings of Taylor and Stephens (1998). JDS estimate a range in the decadal signal of Stream position of 100 km between 75° W and 55° W. The smaller range at A-10 is consistent with the composite of Gulf Stream positions given in JDS that shows a wider envelope of Stream paths east of 72° W.

CM describe a correlation between the NAO and Gulf Stream transport at multi-decadal time-scales (high [low] NAO index, high [low] transport). JDS discuss a correlation between the NAO and the Gulf Stream position on similar time-scales (high [low] NAO index, north [south] position). As illustrated in Figs. 12 and 13, the A-10 records of Gulf Stream transport and position and the NAO index are also approximately in-phase at decadal periods after 1965–1970.

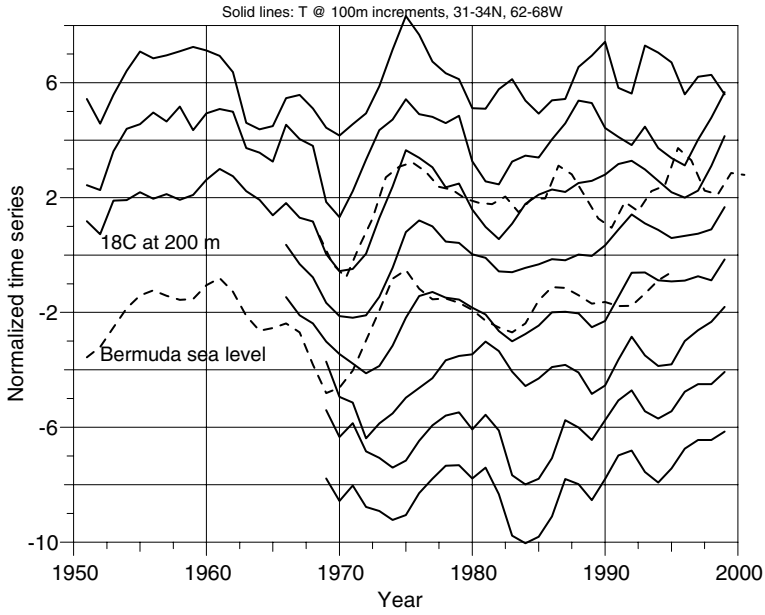

Fig. 15. Temperature time series generated from a 3° by 6° quadrangle surrounding Bermuda (BER in Fig. 1). Solid lines represent normalized, by record length standard deviation, SD, temperature records at 100 m intervals from the surface (top curve) to 700 m (bottom curve). Normalization factors range from about 0.15–0.20 °C in the upper 500 to 0.30–0.35 °C below 500 m. The dashed lines represent Bermuda sea level from Sturges and Hong (1995), SD = 3.2, and the northeastern most position of the 18 °C isotherm at 200 m, SD = 2.38.

Maximum correlation between the longer NAO index and the A-10 Gulf Stream position (Fig. 13), 0.81, occurs when the NAO leads the position by 2-years. Taylor and Stephens (1998) using SST data to define the position of the Stream find a similar lag. JDS estimate maximum correlation between position and NAO at zero lag. However, they computed a modified NAO index using SLP in the subtropics rather than at the Azores as in Hurrell (1995), possibly explaining the lag differences.

The easternmost position of the 18 °C (16 °C) isotherm at 200 m (400 m) and north of 35° N is used to provide a measure of the decadal variability in the size of the recirculation gyre south of the Gulf Stream. The 18 °C record includes a decadal signal (Fig. 14). The 16 °C record also includes a decadal signal, which is in phase with the 18 °C time series. However, towards the end of the 16 °C record, the amplitude of the decadal signal is much reduced compared to the amplitude of the 18 °C time series. Fewer data at 400 m (not shown) could be one cause of the amplitude difference. The extension of the 18 °C isotherm is taken as a measure of the size of the recirculation gyre. As with the annual cycles of the WK gyre size and Gulf Stream transport and position, the decadal signals of the gyre and the Stream properties are also essentially in phase (Fig. 14).

XBT data collected in the BER quadrangle show the temporal evolution of the vertical distribution of temperature on decadal time-scales in the vicinity of the southern boundary of the WK recirculation gyre (Fig. 1). At BER, temperature events propagate from the surface to at least 700 m (Fig. 15). For example, a cooling event originates at the surface in 1970 and is observed at 700 m in 1975. Similarly, a 1975 surface-warming signal propagates to 700 m by 1980 and a 1980 cooling event to 700 m by 1984 (Fig. 15). After 1985, noise increases in the temperature series, most likely related to reductions in available data. However, additional events are still discernible (e.g., surface warming in 1988–1990 propagating downward to 700 m in 1992).

The time series of the size of the southern recirculation gyre and temperature records and sea level at BER are given in Fig. 15. As a reminder, the size of the gyre is taken as the northeastern most point of the 18 °C at 200 m. As shown in Fig. 7, this point is found around 40° N and 40° W, Fig. 7, middle panel. Bermuda is located at 32.5° N and 65° W (Fig. 1). Both time series can be taken as representative of the decadal signal in the characteristics of the southern recirculation gyre. The sea level time series (and temperature records) documents the change in the thermal structure in the interior of the recirculation gyre. The intrusion of the 18 °C isotherm documents the eastward extent of the gyre.

The gyre size is correlated with the temperature and sea level records. For instance the 1970 minimum in gyre size coincides with the cooling event (lower sea level) that encompasses the 1970–1975 period. The subsequent increase in gyre size is coincident with the 1975–1980 warming (higher sea level) event. The 1986–1987 extremes in Bermuda sea level, gyre size and temperature records are also visually correlated. Thus, the decadal signal in sea level at Bermuda can be related to events propagating from the west, the recirculation gyre, (i.e., Watanabe et al., 1999) rather than the east, planetary waves (e.g., Sturges & Hong, 1995). However, the relation of the recirculation gyre variability to planetary wave propagation is unknown, thus precluding any definitive statements on the importance of planetary wave activity on the thermal structure in the vicinity of Bermuda.

CM addressed the vertical extent of the multi-decadal signal in the recirculation gyre. They generated a map showing the difference in PEA distribution between periods of low (1965–1974) and high (1990–1997) Gulf Stream transport. CM attribute a portion of the large multidecadal PEA differences in the western Atlantic to anomalies in the recirculation gyre located south of the Gulf Stream. They go on to select three geographic regions where PEA differences are largest. These regions are outlined in Fig. 1, with area BER substituted for area A of CM because of XBT data availability. CM find that the largest changes in PEA with respect to depth in Box B, Fig. 2, occur between about 700 and 1200 m (i.e., below the main thermocline). The three regions of large multidecadal differences are co-located with the WK gyre (Fig. 1) and the total water column gyre described by Stommel et al. (1978). Area C is located in the region taken to represent the northeastern extent of the decadal signal in gyre size (Fig. 7). Thus, the recirculation gyre located south of the Gulf Stream varies at time-scales ranging from annual to multi-decadal.

5.4. Sampling considerations

The robustness of the A-10 geostrophic transport calculation relative to 450 m is somewhat limited as the results are dependent on the editing and mapping procedures used to generate this time-series. However, as described above the similarities with the CM transport series indicate that the A-10 transport, Fig. 12, can provide a realistic picture of upper layer Gulf Stream transport variability on decadal time-scales.

At zero time lag, the longer overlapping JDS and A-10 position series in Fig. 13 are correlated at 0.72 at the 95% significance level. Thus, Gulf Stream positions derived from MBT and XBT data collected along the A-10 section are representative of decadal changes in Gulf Stream position along the 2000 km path length used by JDS.

The resolution of the ACCE profiling float array (Fig. 5) is less than the proposed 3° resolution for the long-term float array, Argo, http://argo.jcommops.org/. However, even at reduced numbers, the float array is able to resolve the spatial characteristics of the mean bimonthly gyre size developed from the XBT data (Fig. 16). Differences are typically within the uncertainties incurred by mapping the data onto a 2-degree grid.

The mean annual position of the 18 °C isotherm at 200 m has also been derived from the float data and is compared to the same isotherm derived from XBT data for the years of concurrent data, 1998–2001 (Fig. 17). Although the period of overlapping observations is short, the float data reproduces the interannual variability observed in the XBT measurements during this period.

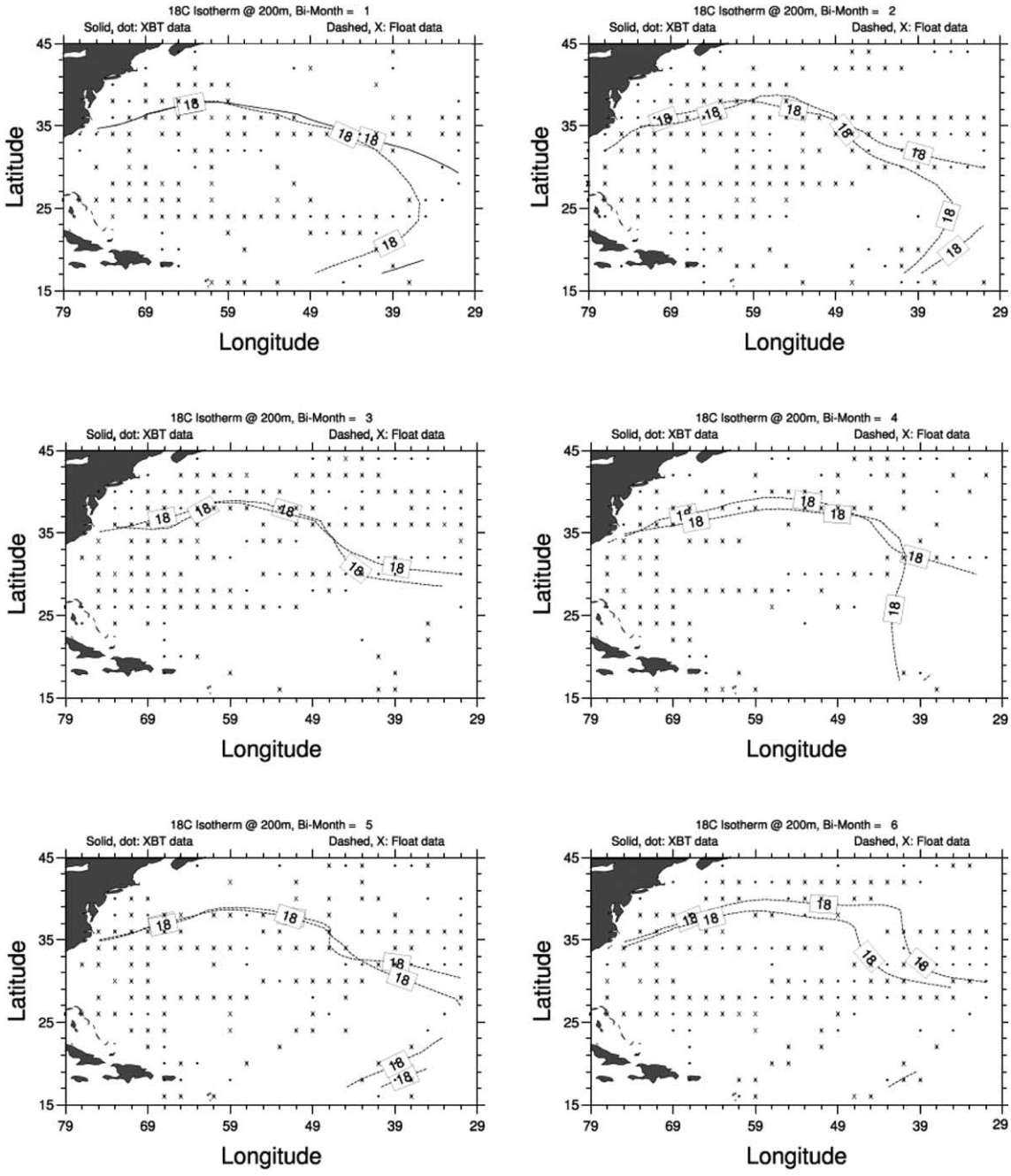

Fig. 16. Comparison of mean bimonthly contours of the 18 °C isotherm at 200 m derived from XBT (solid contours) and profiling float (dashed contours) observations. Data availability on a 2° by 2° grid is also indicated. Bi-month 1 = January–February, Bi-month 2 = March–April, etc. The rms difference between raw and gridded bi-monthly XBT (float) temperature distribution computed over the entire section by the mapping routine is 0.6 (0.9) °C, for bi-month 1; 1.0 (0.9) °C for bi-month 2; 1.0 (1.1) °C for bi-month 3; 1.4 (1.3) °C for bi-month 4; 0.7 (0.9) °C for bi-month 5; and 0.9 (0.9) °C for bi-month 6.

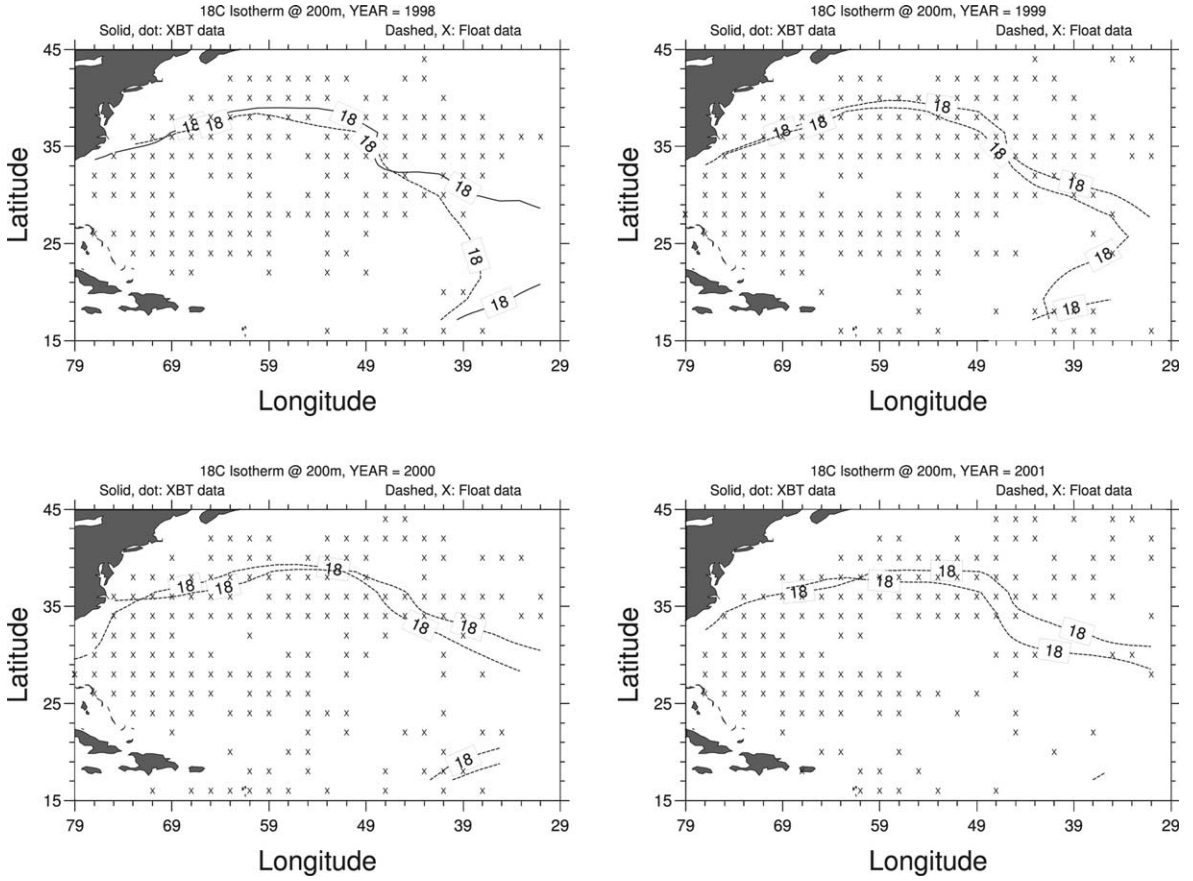

Fig. 17. Comparison of mean annual contours of the 18 °C isotherm at 200 m derived from XBT (solid contours) and profiling float (dashed contours) observations for four years with float data. Data availability on the 2° by 2° grid is also indicated. The rms difference between raw and gridded annual XBT (float) temperature distribution computed over the entire section by the mapping routine is 0.9 (0.9) °C for 1998; 1.0 (0.9) °C for 1999; 1.0 (0.9) °C for 2000; and 0.9 (0.9) °C for 2001.

6. Discussion

Uncertainty estimates for the variables discussed in the text are summarized in Table 2. For most of the records, the signal-to-noise ratio is not large. However, confidence in many of the time-series is gained through favorable comparisons with other records derived from different observing methods (e.g., the mean monthly 300 m transport through A-10 and the Kelly (1991) transports, Fig. 10; the A-10 and JDS Gulf Stream positions, Fig. 13; etc.)

6.1. Mean signals

The mean annual transport of the Florida Current at 27° N is 32.0 Sv (Baringer & Larsen, 2001). The sill depth of the Straits of Florida is about 700–800 m. The mean annual geostrophic transport of the upper 300 m through A-10 is 5.5 ± 1.2 Sv. Since the shallow gyre is located east of the separation latitude of the Gulf Stream (Fig. 1), the Florida Current transport is added to the shallow gyre transport to arrive at an expected Gulf Stream baroclinic transport at 72° W above 750 m of 37.5 Sv. The baroclinic transport relative

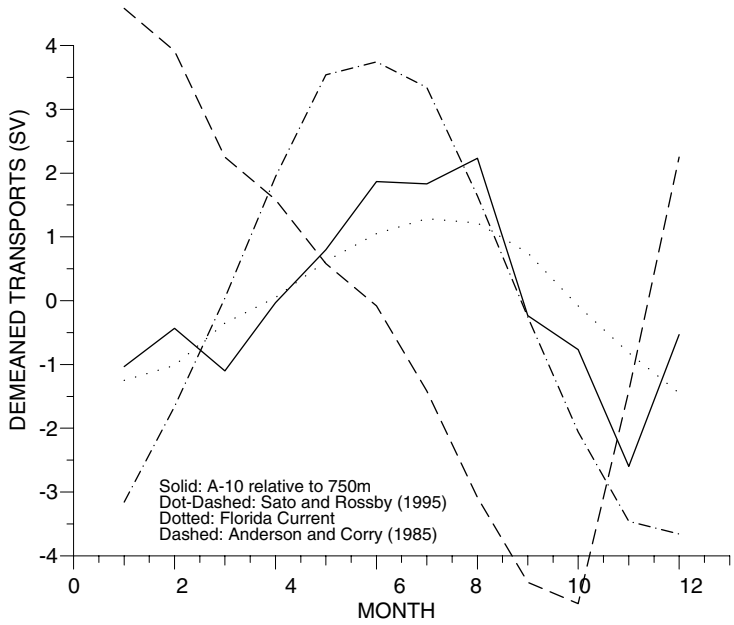

Fig. 18. Demeaned annual cycles of Gulf Stream transport (1) relative to 2000 m from Sato and Rossby (1995), mean = 71.4 Sv; (2) relative to 750 m, through A-10, mean = 36.1 Sv; (3) at 35° N, 70° W from the model of Anderson and Corry (1985), mean = 2.91 Sv and (4) in the Straits of Florida at 27° N, mean = 32.0. All records were smoothed with a 3-month boxcar filter except for the Sato and Rossby (1995) time series, which is filtered with an annual harmonic.

to 750 m derived from the results of this study (Hogg, 1992) is 36.0 ± 3.4 (39.1) Sv. These differences are less than 10% suggesting little change in the total mean baroclinic transport between the Straits of Florida and A-10 above 750 m, except for the addition of the transport related to the shallow recirculation gyre.

6.2. Annual signals

Anderson and Corry (1985) and Böning, Döscher, and Budich (1991) argue that the annual cycle of Florida Current transport is forced primarily by winds within and to the northeast of the Straits of Florida. In contrast, Sato and Rossby (1995) note that the annual baroclinic signal above 2000 m at 73° W "has a gyre wide origin and not just a local response (e.g., Anderson & Corry (1985))". A time-dependent Sverdrup forcing by the surface wind stress curl field east of the mid-Atlantic Ridge (MAR) will not force a baroclinic annual signal in western boundary current transports (e.g., Anderson & Corry, 1985; Böning et al., 1991). A baroclinic signal with annual period is only possible along the western boundary if forced by winds to the west of the MAR as found by Lee, Johns, Zantopp, and Fillenbaum (1996) in a comparison of direct velocity observations along 26.5° N east of the Bahamas with Sverdrup forcing.

The annual cycle of baroclinic transports above 750 m at A-10 and 2000 m at 73° W and the Florida Current transports are out of phase with the results of the linear model of Anderson and Corry (1985) as shown in Fig. 18. The Anderson and Corry (1985) annual cycle in simulated Gulf Stream transport is primarily established by Sverdrupian dynamics and displays a maximum transport in winter. Thus, unlike the results of Lee et al. (1996) at 26.5° N, it would appear that simple time-dependent Sverdrup dynamics are unable to explain the annual cycle of baroclinic Gulf Stream transport after it separates from the coast.

However, Böning, Döscher, and Isemer (1991) show that the form of the annual cycle in boundary current transport at 32° N is strongly dependent on the wind field used in the time-dependent Sverdrup calcu-

lations. The annual cycle they compute from the Hellerman and Rosenstein (1983) winds is very similar to the Anderson and Corry (1985) annual signal shown in Fig. 18. The annual cycle computed from the wind stress climatology of Isemer and Hasse (1987) (in which different drag coefficients and Beaufort equivalencies were used) has a maximum in transport that extends from December through July. Thus, the Isemer and Hasse (1987) winds can explain the summer maximum in observed transport at A-10 but not the winter minima (Fig. 18). Additional analyses are needed to resolve the differences between model and observations.

The shallow recirculation gyre defined by WK overlies the total water column gyre described by Stommel et al. (1978), Fig. 1. WK define the vertical extent of the shallow gyre by comparing EOF representations of the feature derived from satellite and in situ data. They find that the gyre extends to the depth of the annual cycle of temperature generated by surface fluxes (i.e., approximately 200–300 m, south of the Gulf Stream).

WK found that the horizontal spatial structure of the EOF that characterizes the shallow recirculation gyre (Fig. 1) is such that its annual cycle is correlated to seasonal changes in upper layer Gulf Stream transport and position. WK attributed the annual cycle in the size of the shallow recirculation gyre and thus the Gulf Stream properties to forcing by air–sea fluxes. However, because of "large uncertainties in the annual cycle component of the net air–sea heat flux" estimates they use, they cannot close the buoyancy budget. On 5–9-month time-scales, Kelly et al. (1996) find that the surface fluxes west of 62° W are correlated with Gulf Stream transport and, as discussed in the Background section, with the size of the southern recirculation gyre. The BT analyses verify the WK phasing of the annual cycle of the gyre size, shallow Gulf Stream transport and position (Fig. 10) and the near surface location of this feature (Fig. 11). The last result, in particular, supports the WK argument for a surface flux contribution to the annual cycle in the size of the gyre. However, as noted by WK improved estimates of surface fluxes are needed before this relationship can be confirmed quantitatively.

6.3. Decadal signals

Both the A-10 Gulf Stream geostrophic transport relative to 450 m and position time series are essentially in phase with each other and similar signals given by CM and JDS, respectively (Figs. 12 and 13). The Gulf Stream records, particularly after 1965–1970, are also closely in phase with the NAO and the size of a recirculation gyre south of the Gulf Stream (Figs. 12–14). The time series are all characterized by large decadal signals after 1965–1970. The decadal signals are all superimposed on increasing trends.

The spatial structure of the decadal signal of the recirculation gyre indicates that it is co-located with the shallow WK gyre and thus the deeper total water column gyre. Specifically, the isotherm distributions given in Fig. 19 show that the intrusion and retraction of the gyre overlays the EOF representation of the shallow gyre. The decadal signal extends to at least 700 m (Fig. 15). CM find that a multi-decadal signal in the gyre size extends to at least 2000 m. The relation between the decadal and multi-decadal signals has not been quantified. Thus, it is not possible with the XBT data and the CM results to define the vertical extent of the decadal signal beyond 700 m.

Many of the hypotheses generated to explain the decadal signals have been summarized in the Background section. The question now addressed is, do any of these theories or numerical models explain these signals? First, however, it should be noted that positive identification of both the forcing functions for decadal signals and the degree of air–sea coupling is hindered by complicating factors that include: (1) the shortness and paucity of the observational record (Table 1); (2) the apparent non-stationarity of the decadal signals, in most time series they are dominant only after 1965–1970 (Figs. 12 and 13); (3) the small signal to noise ratios in most of the time series considered (Table 2) and (4) possible interactions between anthropogenic and natural variability at these time-scales. However, with respect to non-stationarity, Häkkinen

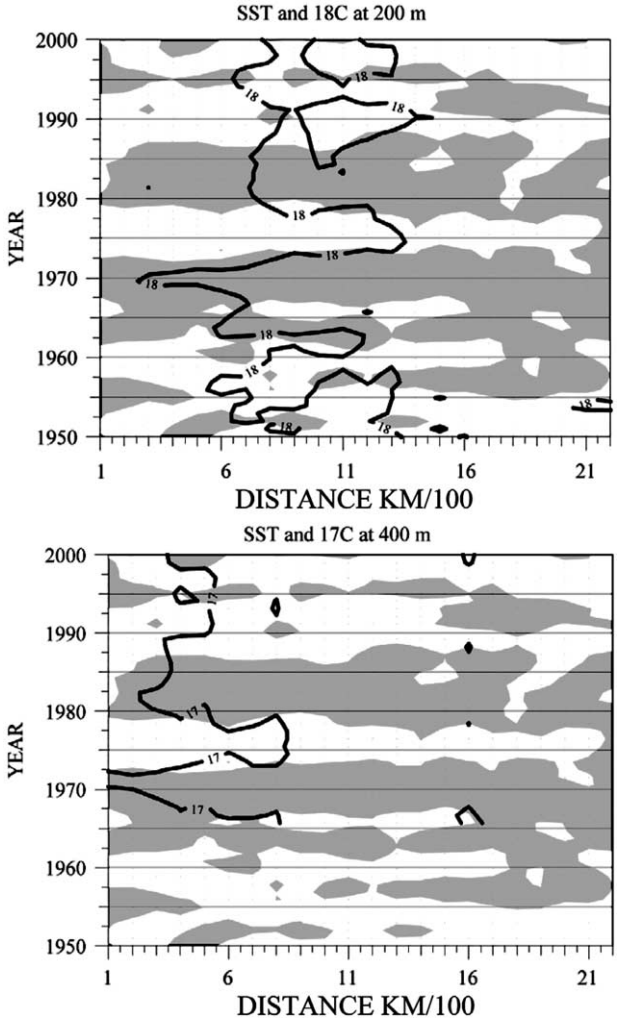

Fig. 19. Upper panel: SST anomalies along the line between the start and year 3 of the Sutton and Allen (1997) correlation line shown in Fig. 1 and the trace of the 18 °C isotherm at 200 m taken to represent the size of the recirculation gyre south of the Gulf Stream. The rms difference between the raw and mapped SST anomalies computed over the entire domain by the mapping routine is 0.06 °C. The rms difference between the raw and mapped temperature fields at 200 m (from which the 18 °C isotherm is extracted) is 0.17 °C. Lower panel: Same as upper panel except for the trace of the 17 °C trace at 400 m. The 17 °C isotherm begins at 1968 because the MBT data do not extend to 400 m. The rms difference between the raw and mapped temperature fields at 400 m (from which the 17 °C isotherm is extracted) is 0.20 °C.

(2000) found robust decadal signals in sea-level records from the southeastern US extending over the last 75 years (i.e., pre 1960s). She argued that these records give "credibility to the existence of a decadal mode".

A theme repeated in the model studies of decadal variability has been the attribution of the decadal signals to variability in the subtropical gyre caused at least in part by the westward propagation of planetary waves and associated upper layer temperature signals from the east. The planetary waves are generated by anomalies in the wind stress curl in the eastern basin (e.g., Sturges & Hong, 1995; Groetzner et al., 1998; Ezer, 1999). However, using observed temperature data collected along 32.5° N (the approximate latitude

of Bermuda) Watanabe et al. (1999) find eastward propagation of temperature anomalies in the upper 100 m and westward propagation only below this layer. Thus, they argue that the surface and subsurface layers are decoupled and planetary wave propagation is unlikely to cause the SST signals required for phase shifting in the decadal modes at these subtropical latitudes. They argue that surface layer advection rather than planetary wave propagation is responsible for the SST role at decadal periods.

Surface layer advection associated with the recirculation gyre located south of the Gulf Stream could provide the mechanism needed to explain the decadal signals in regional SST distribution, sea level at Bermuda and Gulf Stream position and transport. SA (1997) determined areas of maximum correlations between SST just east of Cape Hatteras and downstream in the Gulf Stream/North Atlantic Current region. Annual regions of this correlation were mapped and showed a nine-year period of propagation from the east coast of North America into the North Atlantic Current. The center of each annual area has been estimated from Fig. 1b of SA. The points are displayed in Fig. 1 and show that the SST anomalies propagate through the center of the shallow gyre reported on by WK and the gyre defined by Kelly et al. (1996).

Distance–time temperature plots have been generated for the portion of the SA correlation line just described between the start and year-3 (Fig. 1) of the record. Data within a 5-degree swath around the line were used in the computations. The distance between the start and end of this line is 2200 km. Temperature distributions at 200 and 400 m were compared to SST to consider possible connections between the propagating signals of SA and the size of the recirculation gyre. Previously, the 18 °C (16 °C) isotherm at 200 m (400 m) was used to define the size of the gyre (Fig. 14). However, because of the wide swath used in the present computations, after some testing, the 17 °C at 400 m was found to provide a better indicator of the gyre size for this comparison.

The SST anomaly field and the trace of the 18 °C (17 °C) isotherm at 200 m (400 m) are given in Fig. 19. The decadal signal at 200 and 400 m in the size of the recirculation gyre (Fig. 13) is correlated with the SST anomaly time series with deep (shallow) intrusions of the 18 °C isotherm coincident with warm (cold) SST anomalies (Fig. 19). Thus, the propagating SST signals of SA and Hansen and Bezdek (1996) are not only a surface feature but extend to at least 400 m. In addition, the SST anomalies are correlated with the decadal signals in the size of the recirculation gyre south of the Gulf Stream. Accurate heat budget calculations are required to quantify precisely the relation between the SST signals and the gyre. The XBT data by themselves, and present surface flux estimates, are inadequate to perform such calculations. Results from models that include the decadal signals of propagating SST anomalies and the size of the recirculation gyre, and have been suitably verified, can provide a mechanism for performing these budget calculations.

Similar to the previous inadequacies, available data are also insufficient to separate the effects of wind forcing and surface heat flux forcing on the decadal signal of gyre variability. As indicated previously, Cushman-Roisin (1987) and Huang (1990), using models with different levels of sophistication, have shown that surface flux forcing can drive anomalies in the southern circulation gyre. Marshall et al. (2001) find that both wind forcing and surface fluxes can cause variability in the characteristics of the southern recirculation gyre. The relative effects of each depend on coupling parameters used in their model. Observationally, Kelly et al. (1996) have a 2.5-year long record of recirculation size. Over that record length the gyre contracted as surface flux forcing weakened and the zero line of the wind stress curl acquired a more northeastward tilt. The Kelly et al. (1996) record was obviously too short to define quantitatively relationships on longer time-scales. Furthermore, as expressed by WK for the case of the annual cycle of the recirculation gyre, quantitative progress will only be made when more accurate wind stress and surface flux distributions become available.

Alternatively, Spall (1996a, 1996b), offers another explanation for decadal variability in Gulf Stream transport and position and the size of the recirculation gyres bracketing the Gulf Stream that is independent of time-dependency in the NAO or planetary wave propagation in the subtropics. The explanation is based

on the results from a three-layer primitive equation model in which the upper layer represents the Gulf Stream, the middle layer, the upper limb of the Deep Western Boundary Current (DWBC) and the bottom layer, lower limb of the DWBC. The model is forced at the surface by steady zonal winds and steady transport through the model boundaries in all three layers.

An oscillation is established in the model that involves the Gulf Stream, the recirculation gyres and the upper limb of the DWBC. Feedbacks between these features can result in self-sustaining oscillations with a decadal period. Specifically, the upper limb of the DWBC interacts with the Gulf Stream to cause changes in Gulf Stream position and transport as well as modifications in the recirculation gyres. During the high-energy state of the oscillation, the Gulf Stream transport increases, the Stream moves north and the recirculation gyres strengthen. If a result of gyre strengthening is an increase in gyre size, than the observed properties of the Stream and southern gyre are in phase with the model (i.e., larger transports and southern gyre and northern Stream position, Fig. 19). There are presently insufficient data on the DWBC to verify this hypothesis.

In summary, the observational results given above provide evidence for a recirculation gyre located south of the Gulf Stream as an important component of decadal variability in the northwestern subtropical Atlantic. The evidence presented indicates that decadal signals in gyre size are correlated with similar period signals in Gulf Stream transport and position. The gyre size is also correlated with the propagation of SST anomalies identified by SA. The observational evidence and modeling results are still inadequate to determine the forcing mechanisms for the oceanic decadal variability. Similarly, the degree of coupling between atmosphere and ocean in this region still remains an open question. The findings present herein, however, do provide rationale for enhanced consideration of recirculation gyres associated with the Gulf Stream in studies of North Atlantic decadal climate variability.

6.4. Sampling implications

Smith et al. (1999) describe the role of XBT sampling in future ocean-observing systems. This role is based on the assumptions that both a complete 3000 Argo float array and a satellite altimetric mission will be in place. The ACCE results demonstrate that the Argo array will be sufficient to monitor at a minimum the temperature changes in the large-scale gyres of the ocean basins. However, it is envisioned that an HD network will still be required to provide increased resolution of upper layer temperature variability as outlined in Smith et al. (1999).

Several other altimetric studies have observed a similar annual cycle of upper layer Gulf Stream transports to that obtained from hydrographic observations given in Fig. 10, with maximum upper layer transports in the fall and minimum in the spring (e.g., Kelly, 1991; Zlotnicki, 1991). These altimetric derived transports are out of phase with those estimated from hydrographic data that use a deeper reference level. The transports referenced to deeper levels exhibit a minimum in fall (Fig. 9). Sato and Rossby (1995) find that the dynamic height signal associated with near-surface steric effects has a larger annual cycle amplitude than the amplitude of the annual cycle associated with thermocline displacements. They note that although the thermocline displacements control transports referenced to deeper levels, the shallower steric effects dominate the signal observed by the satellite altimeter.

Thus, to track deeper changes of Gulf Stream transport, continuation of A-10 is desirable. Since the results of CM indicate that transport changes on decadal time-scales penetrate to at least 2000 m, it would be advantageous to use XBT's that sample to this depth rather than the presently used 450 and 750 m probes. Ultimately, methods will be developed that allow estimation of Gulf Stream transport from the profiling float data either directly or through assimilation into oceanic models. However, even then it would be advantageous to continue occupation of lines like A-10 as they provide long continuous records of upper ocean variability.

Acknowledgements

Comments by Dr. C. Meinen are gratefully acknowledged. Two anonymous reviewers provided important suggestions to improve the manuscript. Roberta Lusic prepared the manuscript for publication.

References

Anderson, D. L. T., & Corry, R. A. (1985). Seasonal transport variations in the Florida Straits: a model study. *Journal of Physical Oceanography, 15*, 773–786.

Baringer, M. O., & Larsen, J. C. (2001). Sixteen years of Florida Current transport at 27N. *Geophysical Research Letters, 28*, 3179–3182.

Battisti, D. S., Bhatt, U. S., & Alexander, M. A. (1995). A modeling study of the interannual variability of the North Atlantic Ocean. *Journal of Climate, 8*, 3067–3083.

Bjerknes, J. (1964). Atlantic air–sea interaction. *Advances in Geophysics*. New York: Academic Press, pp. 1–82.

Böning, C. W., Döscher, R., & Budich, R. G. (1991). Seasonal transport variation in the western subtropical North Atlantic: experiment with an eddy-resolving. *Journal of Physical Oceanography, 21*, 1271–1289.

Böning, C. W., Döscher, R., & Isemer, H.-H. (1991). Monthly mean wind stress and Sverdrup transport in the North Atlantic: a comparison of the Hellerman–Rosenstein and Isemer–Hasse climatologies. *Journal of Physical Oceanography, 21*, 221–235.

Conkright, M. E., Locarnini, R. A., Garcia, H. E., O'Brien, T. D., Boyer, T. P. & Stephens, C., et al. (2002). *World Ocean Atlas 2001: Objective Analyses, Data Statistics and Figures*. CD-ROM Documentation, National Oceanographic Data Center, Silver Spring, MD. 17 pp.

Cushman-Roisin, B. (1987). On the role of heat flux in the Gulf Stream-Sargasso Sea subtropical gyre system. *Journal of Physical Oceanography, 17*, 2189–2202.

Curry, R. G., & McCartney, M. S. (2001). Ocean gyre circulation changes associated with the North Atlantic Oscillation. *Journal of Physical Oceanography, 12*, 3374–3400.

Daneshzadeh, Y. H., Festa, J. F., & Minton, S. M. (1994). *Procedures used at AOML to quality control real time XBT data collected in the Atlantic Ocean*. NOAA Technical Memorandum, AOML-78, 44 pp.

Davis, R. E., Webb, D. C., Regier, L. A., & Dufour, J. (1992). The autonomous Lagrangian circulation explorer (PALACE). *Journal of Atmospheric and Oceanic Technology, 9*, 264–285.

Delworth, T. L., & Mann, M. E. (2000). Observed and simulated multidecadal variability in the Northern Hemisphere. *Climate Dynamics*(16), 661–676.

Deser, C., & Blackmon, M. L. (1994). Surface climate variations over the North Atlantic during winter: 1900–1989. *Journal of Climate, 6*, 1743–1753.

Eden, C., & Jung, T. (2001). North Atlantic interdecadal variability: Oceanic response to the North Atlantic Oscillation (1865–1997). *Journal of Climate, 14*, 676–691.

Emery, W. J., & Dewar, J. S. (1982). Mean temperature–salinity, salinity–depth and temperature–depth curves for the North Atlantic and the North Pacific. *Progress in Oceanography, 11*, 219–305.

Ezer, T. (1999). Decadal variabilities of the upper layers of the subtropical North Atlantic: an ocean model study. *Journal of Physical Oceanography, 12*, 3111–3124.

Festa, J. F., & Molinari, R. L. (1992). An evaluation of the WOCE voluntary observing ship XBT network in the Atlantic Ocean. *Journal of Atmospheric and Oceanic Technology, 9*, 305–317.

Frankignoul, C., Muller, P., & Zorita, E. (1997). A simple model of the decadal response of the ocean to stochastic wind forcing. *Journal of Physical Oceanography, 27*, 1533–1546.

Groetzner, A., Latif, M., & Barnett, T. P. (1998). A decadal climate cycle in the North Atlantic Ocean as simulated by the ECHO and coupled GCM. *Journal of Climate, 11*, 831–847.

Häkkinen, S. (2000). Decadal air–sea interaction in the North Atlantic based on observations and modeling results. *Journal of Climate, 13*, 1195–1219.

Halkin, D., & Rossby, T. (1985). The structure and transport of the Gulf Stream at 73W. *Journal of Physical Oceanography, 15*, 1439–1452.

Hansen, D. V., & Bezdek, H. F. (1996). On the nature of decadal anomalies in North Atlantic sea surface temperature. *Journal of Geophysical Research, 101*, 8749–8758.

Hellerman, S., & Rosenstein, M. (1983). Normal monthly wind stress over the World Ocean with error estimates. *Journal of Physical Oceanography, 13*, 1093–1104.

Hogg, N. G. (1992). On the transport of the Gulf Stream between Cape Hatteras and the Grand Banks. *Deep-Sea Research, 39*, 1231–1246.

Huang, R. X. (1990). Does atmospheric cooling drive the Gulf Stream recirculation. *Journal of Physical Oceanography, 20*, 751–757.
Hurrell, J. W. (1995). Decadal trends in North Atlantic Oscillation regional temperatures and precipitation. *Science, 23*, 665–668.
Isemer, H.-J., & Hasse, L. (1987). *The Bunker climate atlas of the North Atlantic Ocean. Air–Sea Interactions* (Vol. 2). Berlin: Springer-Verlag, p. 256.
Johns, W. E., Shay, T. J., Bane, J. M., & Watts, D. R. (1995). Gulf Stream structure, transport, and recirculation near 68W. *Journal of Geophysical Research, 100*, 817–838.
Joyce, T. M., Deser, C., & Spall, M. A. (2000). The relation between decadal variability of Subtropical Mode Water and the North Atlantic Oscillation. *Journal of Climate, 13*, 2550–2569.
Kelly, K. A. (1991). The meandering Gulf Stream as seen by the Geosat altimeter: Surface transport, position and velocity variance from 73 to 46° W. *Journal of Geophysical Research, 96*, 16721–16738.
Kelly, K. A., Caruso, M. J., Singh, S., & Qiu, B. (1996). Observations of atmosphere–ocean coupling in midlatitude western boundary currents. *Journal of Geophysical Research, 101*, 6295–6312.
Kessler, W. S. (1990). Observations of long Rossby waves in the northern tropical Pacific. *Journal of Geophysical Research, 95*, 5183–5217.
Kushnir, Y. (1994). Inter-decadal variations in the North Atlantic Sea surface temperature and associated atmospheric climate. *Journal of Climate, 7*, 141–157.
Lee, T. N., Johns, W. E., Zantopp, R. J., & Fillenbaum, E. (1996). Moored observations of western boundary current variability and thermocline circulation at 26.5N in the subtropical North Atlantic. *Journal of Physical Oceanography, 26*, 962–983.
Lozier, M. S., Owens, W. B., & Curry, R. G. (1995). The climatology of the North Atlantic. *Progress in Oceanography, 36*, 1–44.
Marshall, J., Johnson, H., & Goodman, J. (2001). A study of the interaction of the North Atlantic Oscillation with ocean circulation. *Journal of Climate, 14*, 1399–1421.
Meacham, S. P. (2000). Low-frequency variability in the wind-driven circulation. *Journal of Physical Oceanography, 30*, 269–293.
Meyers, G., Phillips, H., Smith, N., & Sprintall, J. (1991). Space and time scales for optimal interpolation of temperature: Tropical Pacific Ocean. *Progress in Oceanography, 28*, 198–219.
Sato, O. T., & Rossby, T. (1995). Seasonal and low frequency variations in dynamic height anomaly and transport of the Gulf Stream. *Deep –Sea Research, 42*, 149–164.
Smith, N., Harrison, D. E., Bailey, R., Alves, O., Delcroix, T., & Hanawa, K., et al. (1999). The role of XBT sampling in the ocean thermal network. In: N. Smith, C. Koblinsky (Eds.), Proceedings of the First International Conference on The Ocean Observing System for Climate.
Spall, M. A. (1996a). Dynamics of the gulf stream/deep western boundary current crossover. Part I. Entrainment and recirculation. *Journal of Physical Oceanography, 26*, 2132–2168.
Spall, M. A. (1996b). Dynamics of the gulf stream/deep western boundary current crossover. Part II: Low-frequency internal oscillations. *Journal of Physical Oceanography, 26*, 2169–2182.
Sprintall, J., & Meyers, G. (1991). An optimal XBT sampling network for the eastern Pacific Ocean. *Journal of Geophysical Research, 96*, 10539–10552.
Stommel, H., Niiler, P., & Anati, D. (1978). Dynamic topography and recirculation of the North Atlantic. *Journal of Marine Research, 36*, 449–468.
Sturges, W., & Hong, B. G. (1995). Wind forcing of the Atlantic thermocline along 32N at low frequencies. *Journal of Physical Oceanography, 25*, 1706–1750.
Sutton, R. T., & Allen, M. R. (1997). Decadal predictability of North Atlantic sea surface temperature and climate. *Nature, 388*, 563–567.
Taylor, A. H., & Stephens, J. A. (1998). The North Atlantic Oscillation and the latitude of the Gulf Stream. *Tellus, 50A*, 134–152.
Wabba, G., & Wendelberger, J. (1980). Some new mathematical methods for variational objective analysis using splines and cross validation. *Monthly Weather Review, 108*, 1122–1143.
Wang, L., & Koblinsky, C. J. (1996). Annual variability of the subtropical recirculations in the North Atlantic and North Pacific: a Topex/Poseidon Study. *Journal of Physical Oceanography, 26*, 2462–2479.
Watanabe, M., Kimoto, M., Nitta, T., & Kachi, M. (1999). A comparison of decadal climate oscillations in the North Atlantic detected in observations and a couple GCM. *Journal of Climate, 12*, 2920–2940.
White, W. B. (1995). Design of a global observing system for gyre-scale upper ocean temperature variability. *Progress in Oceanography, 36*, 169–217.
WOCE Data Products Committee (2002). WOCE Global Data, Version 3.0. WOCE International Project Office, WOCE Report No. 180/02, Southampton, UK.
Zlotnicki, V. (1991). Sea level differences across the Gulf Stream and Kuroshio Extension. *Journal of Physical Oceanography, 21*, 599–609.